



LUND UNIVERSITY

Magnetomotive ultrasound for nanomedicine

a mechanistic approach to detection, evaluation and safety assessment

Sjöstrand, Sandra

2021

Document Version:

Publisher's PDF, also known as Version of record

[Link to publication](#)

Citation for published version (APA):

Sjöstrand, S. (2021). *Magnetomotive ultrasound for nanomedicine: a mechanistic approach to detection, evaluation and safety assessment*. Department of Biomedical Engineering, Lund university.

Total number of authors:

1

General rights

Unless other specific re-use rights are stated the following general rights apply:

Copyright and moral rights for the publications made accessible in the public portal are retained by the authors and/or other copyright owners and it is a condition of accessing publications that users recognise and abide by the legal requirements associated with these rights.

- Users may download and print one copy of any publication from the public portal for the purpose of private study or research.
- You may not further distribute the material or use it for any profit-making activity or commercial gain
- You may freely distribute the URL identifying the publication in the public portal

Read more about Creative commons licenses: <https://creativecommons.org/licenses/>

Take down policy

If you believe that this document breaches copyright please contact us providing details, and we will remove access to the work immediately and investigate your claim.

LUND UNIVERSITY

PO Box 117
221 00 Lund
+46 46-222 00 00

Magnetomotive ultrasound
for nanomedicine
a mechanistic approach to detection,
evaluation and safety assessment

Sandra Sjöstrand



LUND
UNIVERSITY

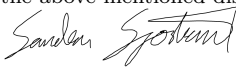
DOCTORAL DISSERTATION

by due permission of the Faculty of Engineering, Lund University.
Public defence on December 16th 2021 at 9:15 in room E:1406, Ole
Römers väg 3, 223 63 Lund, Sweden.

Faculty opponent
Professor Lars Hoff

Organization LUND UNIVERSITY Department of Biomedical Engineering Box 118 SE-221 00 LUND Sweden		Document name DOCTORAL DISSERTATION	
		Date of disputation 2021-12-16	
Author(s) Sandra Sjöstrand		Sponsoring organization	
Title and subtitle Magnetomotive ultrasound for nanomedicine: a mechanistic approach to detection, evaluation and safety assessment			
Abstract Cancer is one of the leading causes of death worldwide, but reliable diagnosis and staging can contribute to optimal treatment planning, and is a crucial factor in reducing mortality and maintaining quality of life. Soft tissue mechanical properties are promising indicators of cancer that can be assessed non-invasively using functional imaging. Additionally, lymphatic involvement is considered a key aspect in staging of many types, including colorectal and breast cancer. Magnetomotive ultrasound, MMUS, is an imaging technique proposed for cancer staging and treatment. It relies on magnetically induced motion, transferred from a contrast agent to the tissue of interest. The tissue response to this perturbation is related to its mechanical properties, and thereby to cancer progression. Typically, the contrast agent consists of magnetic nanoparticles; These can be incorporated into microbubbles, that could allow for drug transport and site-specific delivery. Exploring these properties and possibilities of MMUS clarifies its clinical potential. The aim of this work was therefore to examine (a) the relation between tissue mechanical properties and magnetomotion, (b) the feasibility of magnetic microbubbles as a contrast agent and (c) the cellular response to magnetic nanoparticles and forces. Points (a) and (b) were addressed by comparing MMUS images conducted on real and phantom tissue to finite element analysis outputs; Transmission electron microscopy and quantitative cell based assays were used in exploring point (c). Magnetomotion was found to depend on tissue compressibility and elasticity, both potential cancer indicators. Tissue elasticity was also found to affect the tissue deformations induced by magnetic microbubbles. Furthermore, lymphatic drainage of magnetic microbubbles was demonstrated, validating their potential as a contrast agent in cancer imaging. Finally, cells were confirmed to take up nanoparticles, and no adverse effects of magnetic excitation was detected. In summary, there is merit to further development of MMUS for cancer diagnostics and treatment.			
Key words Magnetomotive, ultrasound, finite element analysis, cancer diagnosis, HT-29, Caco-2			
Classification system and/or index terms (if any)			
Supplementary bibliographical information ISRN: LUTEDX/TEEM-1126-SE, Report No. 4/21		Language English	
ISSN and key title		ISBN 978-91-8039-095-8 (print) 978-91-8039-096-5 (pdf)	
Recipient's notes		Number of pages 65	Price
		Security classification	

I, the undersigned, being the copyright owner of the abstract of the above-mentioned dissertation, hereby grant to all reference sources the permission to publish and disseminate the abstract of the above-mentioned dissertation.

Signature 

Date 2021-11-16

Just keep swimming
-Dory

Advisors

Professor Tomas Jansson
Biomedical Engineering, Department of Clinical Sciences Lund, Lund University, Lund,
Sweden & Clinical Engineering Skåne, Digitalisering IT/MT, Skåne Regional Council,
Lund, Sweden

Doctor Maria Evertsson
Biomedical Engineering, Department of Clinical Sciences Lund, Lund University, Lund,
Sweden

Docent Ingrid Svensson
Department of Biomedical Engineering, Lund University, Lund, Sweden

Doctor Magnus Cinthio
Department of Biomedical Engineering, Lund University, Lund, Sweden

Faculty opponent

Professor Lars Hoff
Department of Microsystems, University of South Eastern Norway, Kongsberg, Norway

Examination committee

Docent Dmitry Grishenkov
Department of Biomedical Engineering and Health Systems, KTH Royal Institute of
Technology, Stockholm, Sweden

Docent Matilda Larsson
Division of Biomedical Imaging, KTH Royal Institute of Technology, Stockholm, Sweden

Docent Elin Trägårdh
Skåne universitetssjukhus, Malmö

Deputy member: Docent Nina Reistad
Department of Physics, Lund University, Lund, Sweden

Chairman

Associate Professor Johan Nilsson
Department of Biomedical Engineering, Lund University, Lund, Sweden

Cover illustration front:

Waves by Anna-Sofia Wiking

ISBN: 978-91-8039-095-8 (print)

ISBN: 978-91-8039-096-5 (pdf)

ISRN: LUTEDX/TEEM-1126-SE

Report No. 4/21

Printed in Sweden by Tryckeriet i E-huset, Lund University, Lund 2021

© Sandra Sjöstrand 2021

Contents

List of publications	iii
Acknowledgements	vii
Popular summary in English	ix
Populärvetenskaplig sammanfattning på svenska	xi
Glossary	xiii
1. Introduction	1
1.1 An overview of relevant magnetic principles	4
1.2 Magnetomotive ultrasound	9
1.3 Tissue mechanical properties	10
1.4 Microbubbles and their magnetic functionalization .	12
1.5 Cellular response	16
2. Aims	21
3. Materials and methods	23
3.1 Tissue mimicking materials	23
3.2 Viscoelasticity	24
3.3 Finite element analysis	25
3.4 Magnetomotive ultrasound	27
3.5 Cell-based assays	27
4. Results and comments	29
5. Implications and Outlook	35
6. References	37
Research papers	45
Authors contributions	45

List of publications

This thesis is based on the following publications, referred to by their Roman numerals:

- I **Tuning viscoelasticity with minor changes in speed of sound in an ultrasound phantom material**
S. Sjöstrand, B. Meirza, L. Grassi, I. Svensson, L. Camargo, T. Pavan, M. Evertsson
Ultrasound in Medicine & Biology, Volume 46, issue 8, pp. 2070–2078, August 2020
- II **Displacement Patterns in Magnetomotive Ultrasound Explored by Finite Element Analysis**
S. Sjöstrand, M. Evertsson, E. Atile, R. Andersson, I. Svensson, M. Cinthio, T. Jansson
Ultrasound in Medicine & Biology, in press
- III **Modelling of magnetic microbubbles to evaluate contrast enhanced magneto-motive ultrasound in lymph nodes – a pre-clinical study**
S. Sjöstrand, M. Bacou, K. Kaczmarek, M. Evertsson, I. Svensson, A. Thomson, S. Farrington, S. Moug, T. Jansson, C. Moran, H. Mulvana
Submitted
- IV **Evaluation of cellular response in magnetomotive ultrasound**
S. Sjöstrand, K. Zeller, M. Evertsson, T. Jansson
Manuscript in preparation

All papers are reproduced with permission of their respective publishers.

Publications produced during the PhD not included in this thesis:

Magnetomotive Ultrasound Imaging Systems: Basic Principles and First Applications

S. Sjöstrand, M. Evertsson, T. Jansson

Ultrasound in Medicine & Biology, Volume 46, Issue 10, pp. 2636–2650, October 2020

Extending imaging range in magnetomotive ultrasound with tailored magnetic nanoparticles

M. Evertsson, **S. Sjöstrand**, TC. Kranemann, A. Mousavi, I. Svensson, M. Cinthio, T. Jansson

IEEE International Ultrasonics Symposium 2020, Proceedings

Construction of an ultrasound phantom with micrometer-sized wall-less vessels

B. Meirza, H. Hasegawa, M. Evertsson **S. Sjöstrand**, M. Cinthio

IEEE International Ultrasonics Symposium 2019, Proceedings

Contrast-enhanced magnetomotive ultrasound imaging (CE-MMUS) for colorectal cancer staging: Assessment of sensitivity and resolution to detect alterations in tissue stiffness

S. Sjöstrand, M. Evertsson, C. Thring, M. Bacou, S. Farrington, S. Moug, C. Moran, T. Jansson, H. Mulvana

IEEE International Ultrasonics Symposium 2019, Proceedings

Revolving permanent magnet causes rotating particle motion that makes new detection schemes possible in magnetomotive ultrasound

M. Evertsson, **S. Sjöstrand**, T. Erlöv, I. Svensson, R. Andersson, M. Cinthio, T. Jansson

IEEE International Ultrasonics Symposium 2019, Proceedings

**Revolving Permanent Magnet for Magnetomotive
Ultrasound**

S. Sjöstrand, M. Evertsson, U. Lindquist, R. Lindkvist, R. Andersson, A. Wahlström, G. Nybom, I. Svensson, M. Cinthio, T. Jansson
IEEE International Ultrasonics Symposium 2018, Proceedings

**Design and fabrication of a conceptual arterial ultrasound
phantom capable of exhibiting longitudinal wall movement**

S. Sjöstrand, A. Widerström, Å. Rydén Ahlgren, M. Cinthio
IEEE Transactions on Ultrasonics, Ferroelectrics, and Frequency
Control, Volume 64, Issue 1, pp. 11 – 18, August 2016

Acknowledgements

This project has been a journey and I would like to thank everyone who came along for any length of it. To my supervisors, Tomas Jansson, Ingrid Svensson, Maria Evertsson and Magnus Cithio who, for offering me this position, helping me grow and staying with me for the whole trip. Also thanks to Kathrin Zeller for helping me develop new skills in the cell lab directing me in this uncharted territory.

To current and former members of the excellent team I had the privilege to work with in Scotland including Susan Moug, Susan Farrington, Helen Mulvana and Carmel Moran for making me feel like part of the team.

All of the above are also co-authors, so I want to thank you in this capacity too, along with Marion Bacou, Lorenzo Grassi, Benjamin Meirza, Theo Pavan, Luciana Camargo, Roger Andersson et al. for that opportunity.

To all of my friendly co-workers in the departments I've been active, and especially to Nebojša Malešević, Axel Tojo, Johan Gran, Aastha Sobti, Lavanya Lokhande, Nico Fenu, Mathew Wilkie-Holland and many more who have the kind of energy that make a workplace better, I congratulate your current and future work-mates. Leif Sörnmo, my mentor who has been a great support and an asset when it comes to navigating academic life, data analysis and the works of Tove Jansson. Thanks to Pontus Kjellman, Peter Jönsson and Ola Gustafsson for sharing your respective expertise in nanoparticle fabrication, physical chemistry and transmission electron microscopy.

There has also been a bunch of bachelor and master's students over the years that I've co-supervised. Thanks for the time, energy and creativity you put in, it has been great to be part of your projects.

Trying to tie back to the journey metaphor, I need to thank the members

of LGBTQ-lu for all kinds of fun and interesting stuff that we got up to along the way.

I also want to acknowledge my closest friends and family, including Sara Saleh, Astrid Görtz, Gunnar Weibull and Kajsa Wernerson for just being there, but also for being awesome, and Bengt, Tina, Joakim, and especially Maj-Britt Sjöstrand for our discussions relating to this project and other things that are important.

Finally, a huge thanks to Natalie Isaksson, for being my sounding board, editor, reviewer 2, biggest fan and inspiration, spouse, and many other things that I needed to complete this epic journey.

Popular summary in English

For many forms of cancer, fast and reliable diagnoses are vital. Even for more benign forms, quick and accurate diagnoses make a big difference to a patients' quality of life and well-being. Medical images are important tools in cancer diagnostics, and there are many methods to obtain such images both used currently and under development. One method that is still in a pre-clinical phase is magnetomotive ultrasound, or MMUS. Using MMUS it is possible to image a contrast agent consisting of magnetic nanoparticles that have been introduced into the body. These kinds of particles can be directed to specific targets in the body, and can also be imaged using whole body imaging techniques (e.g. MRI). The advantage of ultrasound over these techniques is that it is widely available, generates images in real-time during the examination, and is relatively inexpensive. However, the particles are too small to be imaged directly by ultrasound, so MMUS works by using magnets to make the region containing magnetic particles move and imaging this motion. The properties of the particles, as well as of the surrounding tissue determine the propagation of the motion, which means that under certain conditions MMUS can also image tissue stiffness. This is especially relevant in cancer diagnostics as tissue stiffness is often an indicator of cancer, and therefore MMUS could potentially be used to evaluate whether therapy was successful.

To explore in more detail how the properties of MMUS could be useful in cancer diagnostics, I looked at how tissue stiffness and type of contrast agent affect tissue motion and MMUS images, and evaluated safety of the force driving the magnetic motion in cultured cells.

To better understand the relevant mechanical and acoustic properties that govern the motion and ultrasound signal in MMUS, I characterized a tissue mimicking material. The material was composed of two kinds of gels, and interestingly, the elasticity was found to depend on the composition, but

the speed of sound was relatively constant. Since constant speed of sound is usually assumed when building up an ultrasound image, this property could be useful to uphold that assumption while having different elasticity in different regions.

I then predicted motion due to a magnetic force in a simulation model using mechanical data. The modelling was compared to actual MMUS images collected from both a tissue mimic and real tissue. I found that the images have different features based on the stiffness and also compressibility. Since both of these properties are linked to cancer, the image can therefore contain important diagnostic clues.

I also explored possible advantages of using magnetic bubbles, which are larger than particles and can be imaged with conventional contrast enhanced ultrasound. After experimentally confirming that injected magnetic microbubbles accumulate in the target tissue, I again used modelling to explore the interactions between a magnetic microbubble and tissue. Once again there was a relationship between stiffness and motion that could provide diagnostic information.

Finally, I investigated how human cells react to these magnetic particles in combination with a magnetic force. After all, the cellular response to these conditions predicates the feasibility of clinical trials. In these cultured cells, I was able to show that cells took up particles, and found no evidence that the cells were damaged by the magnetic force acting on the particles.

Pre-clinical research such as my work detailed above, lays the necessary theoretical and experimental foundation before a new method, such as MMUS, can be tested clinically. My research showed that diagnostically relevant information can be obtained from MMUS images, and that accounting for the unique physical properties of the contrast agent and setup is important to do so. I showed how advanced modelling techniques can be combined with experimental data to characterise and explore the MMUS study system, such as assessing the feasibility of using magnetic bubbles instead of particles. Finally, I found no negative effect of magneto-mechanical interactions in terms of the evaluated indicators in these human cells, alleviating patient safety concerns.

Populärvetenskaplig sammanfattning på svenska

Vid många former av cancer är snabba och pålitliga diagnoser av yttersta vikt. Även för mer godartade former kan en tidig och korrekt diagnos innebära en stor skillnad i livskvalitet och välmående. Medicinska bilder är viktiga verktyg inom cancerdiagnostik, och det finns en mängd bildgivande metoder som används kliniskt eller som ännu är under utveckling. En metod som utvecklas är magnetomotoriskt ultraljud, eller MMUS, som är den engelska förkortningen. Med hjälp av MMUS går det att avbilda ett kontrastmedel bestående av magnetiska nanopartiklar i kroppen. Denna typ av partiklar kan tas upp av en specifik vävnad i kroppen, och kan även avbildas med helkroppstekniker så som magnetkamera. Fördelen med ultraljud jämfört med sådana tekniker är att ultraljud är mindre kostsamt och mer lättillgängligt, samt att det genererar bilder i realtid under undersökningen. Dock är partiklarna för små för att avbildas direkt med ultraljud, så vid MMUS används magneter för att sätta området med partiklar i rörelse och sedan avbildas själva rörelsen. Hur rörelsen fortplantar sig beror på partiklarnas, men också vävnadens, egenskaper. Detta innebär att MMUS under vissa förutsättningar kan detektera vävnadsstyvhet. Detta är intressant, i synnerhet i relation till cancer eftersom styv vävnad kan vara en indikation, och MMUS skulle därmed kunna användas för att utvärdera om en behandling fungerar som förväntat.

För att utforska i större detalj hur MMUS skulle kunna användas inom cancerdiagnostik har jag undersökt hur vävnadens och kontrastmedlets egenskaper påverkar magnetrörelsen och MMUS-bilder, samt utvärderat huruvida denna teknik påverkar odlade celler.

Eftersom mekaniska och akustiska egenskaper påverkar rörelsen och ultraljudssignalen i MMUS, utvecklade jag ett vävnadesliknande material med

hänsyn till dessa. Materialet i fråga bestod av två olika geler, och det visade sig intressant nog att elasticiteten berodde på kompositionen, medans ljudhastigheten var relativt konstant. Denna egenskap är intressant eftersom ultraljudsbilder byggs upp under antagandet att ljudhastigheten är densamma. Antagandet kan därmed uppfyllas samtidigt som elasticiteten kan variera mellan olika områden.

Sedan användes uppmätta mekaniska egenskaper för att skapa en matematisk modell i avsikt att simulera magnetrörelse. Genom att jämföra den modellerade rörelsen med verkliga MMUS-bilder från vävnadsliknande material och riktig vävnad, kunde jag knyta vissa kännetecken till vävnadsegenskaper så som styvhet och kompressibilitet. Eftersom båda dessa egenskaper är kopplade till cancer tyder detta på att bilderna kan innehålla viktig diagnostisk information.

Jag undersökte även möjliga fördelar med att använda magnetiska bubblor som kontrastmedel. Bubblorna är större än partiklar, och kan användas som ett konventionellt kontrastmedel för ultraljud, det vill säga även utan magnetrörelse. Efter experimentell verifiering av att de magnetiska mikrobubblorna ansamlas i mål-vävnaden använde jag åter igen modellering för att utforska interaktioner, denna gång mellan en magnetisk bubbla och vävnad. Även här framkom ett förhållande mellan styvhet och rörelse som skulle kunna ge diagnostisk information.

Slutligen undersökte jag hur mänskliga celler reagerar på de magnetiska partiklarna i kombination med en magnetisk kraft. Hur cellerna tolererar detta är avgörande för teknikens säkerhet och vidareutveckling. Jag kunde visa att partiklarna togs upp i odlade celler, och hittade inga bevis på att cellerna tog skada av den magnetiska kraften som verkade på partiklarna. Denna typ av forskning bidrar till att skapa den teoretiska och experimentella grund som krävs innan en ny metod, så som MMUS, kan testas kliniskt. Min forskning visade att diagnostiskt relevant information kan tas fram ur MMUS-bilder, och pekade på vikten av att ta hänsyn till egenskaper hos kontrastmedlet och uppställningen för att kunna komma åt denna information. Jag visade hur modelleringsteknik kan kombineras med experimentell data för att karakterisera och utforska MMUS, och utvärdera magnetiska bubblor som kontrastmedel istället för partiklar. Jag fann heller inga negativa effekter av de magnetiska och mekaniska interaktionerna i levande celler, vilket är positivt för vidareutvecklingen av MMUS ur ett patientsäkerhetsperspektiv.

Glossary

Acronyms and abbreviations

B-field	Magnetic flux density [$kg\ s^2\ A^{-1}$]
CT	Computed Tomography
FEM	Finite Element Method
GMM	Generalized Maxwell Model
GSH	(reduced) glutathione
GSSG	(oxidized) glutathione
H-field	Magnetization field, Magnetic field strength [$A\ m^{-1}$]
LDH	Lactate Dehydrogenase
LN	Lymph Node
M	Magnetization [$A\ m^{-1}$]
MB	Microbubble
MMUS	Magnetomotive Ultrasound
MRI	Magnetic Resonance Imaging
NP	Nanoparticle
PVA	Polyvinyl Alcohol
ROS	Reactive Oxygen Species
SEBS	Styrene-Ethylene-Butylene-Styrene
SPION	Superparamagnetic Iron Oxide Nanoparticle
TEM	Transmission Electron Microscopy

Terms

Single magnetic domain	Small volume of uniform magnetization in any field
Magnetomotion	Motion in solid due to magnetic contrast agent
Magnetophoresis	Magnetic motion on a magnetized particle in fluid

Symbols

ρ	density [$kg\ m^{-3}$]
σ	surface tension [$N\ m^{-1}$]
χ	magnetic susceptibility [unitless]
μ	magnetic permeability [$kg\ m\ s^{-2}\ A^{-2}$]
μ_0	$4\pi \cdot 10^{-7}$ [$kg\ m\ s^{-2}\ A^{-2}$], magnetic permeability of free space
k	$1.380649 \cdot 10^{-23}$ [$J\ K^{-1}$], Boltzmann's constant
ζ	Zeta potential [V]

1. Introduction

Cancer is one of the leading causes of death worldwide¹¹ and the prevalence is expected to rise.⁷⁵ It is characterised by abnormal cell growth in a specific region or tissue that can potentially spread to other parts of the body. Signs and symptoms can be mild, vague or even absent in the early stages of disease, meaning it can go undetected. To reach those who are affected yet asymptomatic, screening can be used to test an at risk group for a specific condition. At present, many types of cancer can be successfully treated, especially when detected at an early stage. Early and accurate diagnoses are vital, and are key to reducing the invasiveness of procedures,⁶⁵ and can make a positive difference to the patients well-being and quality of life. Additionally, these procedures require less resources and therefore put less strain on the healthcare system.

Technical development of medical equipment may contribute to this in multiple ways, and especially medical imaging plays an important part in improved screening, diagnosis and monitoring of disease.⁶⁴ Medical imaging can be categorized as anatomical, functional and molecular based on what is being imaged, see Fig. 1.

Earlier detection of disease is realized either through increased sensitivity of conventional (anatomical) medical imaging systems, or through the development of functional and molecular imaging. This is because local physiological and compositional alterations generally precedes anatomical changes. Furthermore, increased diagnostic information available through functional, molecular or multi-modal imaging enables personalized medicine and can help medical professionals choose the best treatment on a case by case basis.⁴³ Combined therapy and diagnosis,²⁶ is another area where medical imaging technologies are evolving to increase efficiency by shrinking the gap between diagnosis and treatment.

Ultrasound is a competitive alternative to a range of imaging examina-

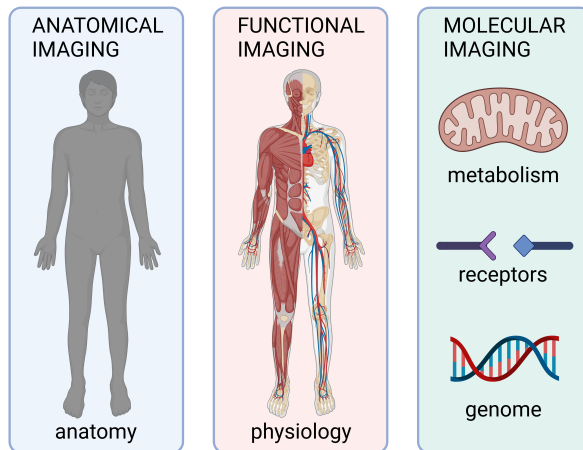


Figure 1: Medical imaging can be categorized based on what is being imaged. Anatomical imaging visualizes the structures such as organs and tissues. Some common examples include computed tomography and magnetic resonance imaging. In functional imaging, the objective is to image physiological activities such as blood perfusion. Some techniques, such as magnetic resonance imaging can provide both anatomical and functional information depending on the type of examination. Molecular imaging can be considered a subset of functional imaging that aims at processes at the cellular or molecular level. It typically involves tracers that accumulate specifically and can be used to monitor increased metabolic rate, molecular receptors and even gene expression. Examples include single photon emission computed tomography and positron emission tomography. Graphic created with BioRender.com

tions, as it provides real-time images, is free from ionizing radiation, widely available and relatively inexpensive. It is a versatile technique, capable of imaging most soft tissues, flow, perfusion and elasticity based on endogenous ultrasound scatterers. With the use of microbubbles as a contrast agent, ultrasound can generate functional images of the vascular system where endogenous contrast is typically low. Molecular imaging is, however, associated with a number of challenges that are difficult to reconcile with conventional contrast enhanced ultrasound imaging. Critical to contrast enhanced molecular imaging is that the agent is able to reach and bind to the target. Conventional ultrasound contrast agents typically consist of micrometer-sized bubbles and that cannot reach most tissues. Contrast enhancement of vascular organs has been achieved with microbubbles, but their size prevents diffusion through the vascular epithelium.⁶

Submicrometer-sized contrast particles, such as perfluorocarbon droplets³⁹

and liposomes have been developed in an attempt to reach extravascular targets. Some of these particles are small enough to migrate through injured or leaky vasculature where the permeability is abnormally high,¹⁴ but since the scattering strength of an insonated particle decreases with the sixth power of the radius of the particle, ultrasound echo-based imaging becomes very challenging.¹⁵ For submicron droplets, this challenge is overcome by harvesting the incoming sound energy to achieve a phase change of the droplet into a bubble, to achieve adequate contrast. Alternatively, there are visualization strategies for contrast agents in nano- to submicrometer size that use ultrasound in combination with other contrast mechanisms.

One such visualization strategy is photoacoustic imaging. In the contrast enhanced case, an agent, e.g. plasmonic particles, creates an ultrasound wave upon thermal expansion induced by pulsed laser radiation.⁸⁰ The same principle of inducing ultrasound waves can also be used with strongly absorbing endogenous molecules, such as hemoglobin.⁷⁸ As with other optic techniques, the penetration depth of photoacoustic imaging is limited by the high scattering of light in tissue.

Another approach considers the use of a magnetic contrast agent. This agent can be put in motion by an external magnetic field and simultaneous detection of the induced movement pinpoints the location of the contrast agent, as illustrated in Fig. 2.

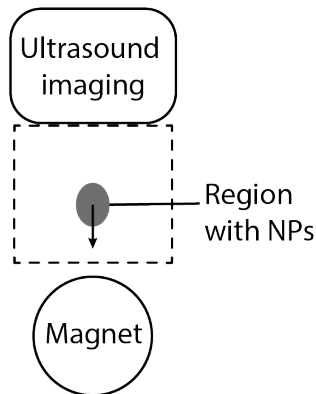


Figure 2: The principle of magnetomotive ultrasound. A region containing magnetic nanoparticles is set in motion by a magnet. While the particles are too small to image directly, the motion can be captured by ultrasound, thereby imaging their presence indirectly.

The technique magnetomotive ultrasound (MMUS),⁵⁴ builds on an optical

coherence technique,⁵⁶ but ultrasound offers deeper tissue penetration as compared to light. MMUS can therefore image deeper targets, such as lymph nodes, that lie at a distance from the surface.

The use of magnetic nanoparticles as a contrast agent could enable ultrasound molecular imaging of extravascular targets. The particles also offer potential for multimodal imaging²² as well as magnetic heating. While the magnetic particles are usually used directly, incorporating them into microbubbles could improve the sensitivity of this technique for suitable targets that bubbles may reach.

The contrast mechanism makes the technique inherently sensitive to variations in tissue mechanical properties, which could be exploited in a type of functional imaging for fine scale elastography. In this thesis, the mechanical action that is generated was investigated in relation to imaging, therapy, diagnosis and safety aspects of MMUS.

The theoretical framework for this investigation will be introduced under a number of subheadings, that lead up to the formulation of the aims in section 1.5. The force acting on the magnetic contrast agent is central to this imaging technique and so an overview of magnetism in this context is presented first, followed by an introduction to MMUS. The mechanical properties of soft tissues are covered since these relate the applied magnetic force to the observed motion, a relation that could be exploited to infer tissue properties. Microbubbles are then briefly discussed as well as possible advantages of magnetic microbubbles as a contrast agent. Finally, the perspective is shifted to the cellular level and how magnetic and mechanical interactions may affect living cells.

1.1 An overview of relevant magnetic principles

Magnetic objects experience attractive or repellent forces when in proximity. The attractive force on magnetic nanoparticles due to an applied, time-varying magnetic (or rather, magnetization) field is fundamental for MMUS. In this section, some of the most relevant theory will be introduced in order to derive an expression for the magnetic driving force.

The interaction between a magnetizing field and magnetic particles engenders energy exchanges. High frequencies, typically hundreds of kHz causes heating,¹⁸ while lower frequencies and a stationary field tend to induce forces that set the particles in motion.⁷ In the current context, the main

interest is magnetic attraction forces acting on magnetic nanoparticles in a field gradient.

This section will describe some suitable field characteristics for this application and how these can be achieved. Furthermore, it will describe the interaction between such a field and an assembly of magnetic nanoparticles. The underlying theory will be discussed in relation to experimental conditions.

Magnetization field

A fundamental component for MMUS imaging is a time-varying magnetic field giving rise to a displacement force. It is challenging to achieve a detectable displacement especially at depth and while limiting the nanoparticle dose according to *in vivo* conditions.

The magnetic force depends both on properties of the particles as well as the field. To derive an expression for the force, some concepts and definitions are needed. The magnetization field, also termed magnetic field strength, \mathbf{H} , in units of $[A\ m^{-1}]$, is established in a region independent of the background medium. \mathbf{H} is related to the magnetic flux density $\mathbf{B}[kg\ s^2\ A^{-1}]$ inside a material by its magnetic permeability $\mu[kg\ m\ s^{-2}\ A^{-2}]$ according to

$$\mathbf{B} = \mu\mathbf{H}. \quad (1)$$

The magnetic permeability of free space μ_0 is a constant equal to $2\pi 10^{-7}$ $[kg\ m\ s^{-2}\ A^{-2}]$. In matter the relative permeability μ_r [dimensionless], is defined as the ratio of the magnetic permeability of that material and the permeability of free space,

$$\mu_r = \frac{\mu}{\mu_0}. \quad (2)$$

As an example, a coil carrying an electric current gives rise to magnetization field \mathbf{H}_c . If the coil is placed in vacuum the resulting magnetic flux density will be given directly by equation 1 with $\mu = \mu_0$. However, if a highly magnetically permeable material such as iron is placed inside the coil, see Fig. 3, the magnetic flux density, \mathbf{B} will be higher. This is because these materials by definition can carry a higher magnetic flux density for a given magnetization field, or, equivalently, μ is higher in equation 1. The magnetic domains inside the iron align with the external field and, as a result, the flux density is increased both inside and outside of the material.¹⁰ An iron core is therefore often used in MMUS to direct and concentrate

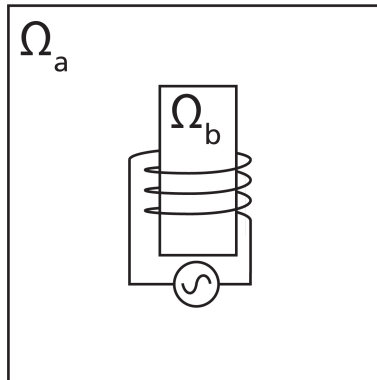


Figure 3: Coil carrying an alternating current as indicated by a encircled wave sign. Placing an iron core Ω_b in the coil changes the magnetic flux density both inside Ω_b as well as in the surrounding medium Ω_a . The surrounding medium is assumed to be homogeneous and non-magnetic in this illustration.

magnetic flux.^{54,21,47,3,38,58} The following sections will explore the interactions that occur when superparamagnetic iron oxide nanoparticles are present within a varying magnetization field.

Field-particle interaction

Superparamagnetic nanoparticles exhibit certain magnetic properties that enable high magnetization in an external field and relaxation when the magnetic field strength decreases. These characteristics are desirable in MMUS and therefore such particles are commonly, but not exclusively,¹² used in this technique.^{54,46,22,3} A particle must be sufficiently small to only contain a single magnetic domain in order for it to exhibit these characteristics and be classified as superparamagnetic.⁸ Fig. 4 shows a simplified model of a single domain particle.

The magnetization \mathbf{M} [$A\text{m}^{-1}$] is defined as the vector sum of magnetic moments \mathbf{m} per unit volume V ,

$$\mathbf{M} = \frac{d\mathbf{m}}{dV}. \quad (3)$$

The magnetization \mathbf{M} contributes to the magnetic flux density \mathbf{B} in a material according to the definition

$$\mathbf{B} \equiv \mu_0(\mathbf{H} + \mathbf{M}). \quad (4)$$

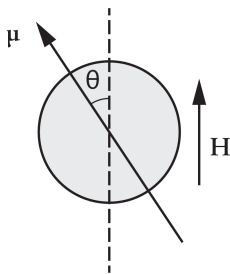


Figure 4: Isotropic single domain particle, adapted from.⁸ Here μ denotes the total magnetic moment of the particle, H is the magnetization field and θ is the angle between those two vectors.

It is because of this contribution that permeability is material dependent, compare also equation 1. The degree of magnetization in response to an applied magnetization field is highly material dependent. The ratio of magnetization to the applied magnetization field is termed magnetic susceptibility and denoted χ . At zero field, the magnetic moments of an assembly of superparamagnetic nanoparticles will be randomly distributed such that the net magnetization is zero. On the other hand, with a strong field the moments will line up and the magnetization reaches its maximum.

The fraction of the magnetization in an assembly of isotropic, single magnetic domain particles aligned by the field follows a characteristic curve, the Langevin function $L(\alpha)$

$$L(\alpha) = \coth(\alpha) - \frac{1}{\alpha}, \quad (5)$$

where $\alpha = \mu H/kT$. Here, k is the Boltzmann constant and T the absolute temperature. This function is approximately linear close to $H = 0$ and asymptotically approaches one as H becomes large.⁸ Saturation occurs because eventually all magnetic moments in the system are aligned. Scaling the function $L(\alpha)$ by the saturation magnetization M_S gives the magnetization curve for a system of particlesⁱ, see Fig. 5.

ⁱThis theory treats an assembly of isotropic, identical and non-interacting particles at thermal equilibrium. For the purpose of introducing the underlying theories and mechanisms, one can assume that all conditions are fulfilled. Under experimental conditions however, the particles will be partially anisotropic and represent a distribution of sizes. Introducing a low degree of anisotropy and size variation has a small effect on the shape of the magnetization curve. This effect is therefore assumed negligible, and the system will be assumed to be at thermal equilibrium throughout. Interaction between neighbouring particles will be treated separately in the section about inter-particle interaction.

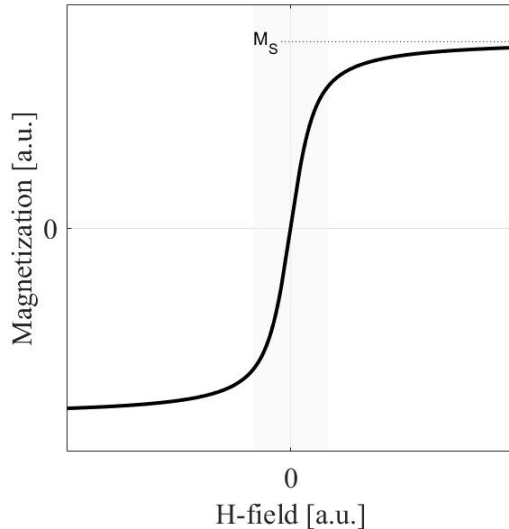


Figure 5: The characteristic Langevin curve for an assembly of isotropic, identical and non-interacting superparamagnetic nano-particles at thermal equilibrium. The curve is approximately linear close to $H = 0$, and approaches M_S when H is large. Both axes are in arbitrary units, a.u.

The magnetization characteristics are needed to evaluate the volumetric force \mathbf{f}_V ,⁵² given by

$$\mathbf{f}_V = \mu_0(\mathbf{M} \cdot \nabla)\mathbf{H} \quad (6)$$

with the gradient operator ∇ . This expression is derived from the Maxwell equations of electromagnetism assuming that the electric field is zero or negligible, $\mathbf{M} \ll \mathbf{H}$ and that the curl is small. Note that the magnetization of the suspension depends on the magnetic properties of the particles as well as the medium. Water based carriers are inherently diamagnetic, meaning they will experience a force directed oppositely to that acting on the (para)magnetic particles.⁵⁵ Diamagnetic materials have a low but constant magnetic susceptibility with a negative sign. Compared to other types of magnetism, diamagnetism is generally weak but not always negligible.

The basic theory of superparamagnetism assumes isotropic, non-interacting particles. The next section briefly explores how particle-particle interactions modifies this theory.

Inter-particle interaction

The moment of each particle has an impact on the magnetic flux density in its immediate surrounding, so particles in close proximity ($\leq 70 \text{ nm}$) sense a lower field than isolated particles.⁷⁶ Under certain conditions, such as multi-core particles or loaded microbubble shells, the proximity of the nearest neighbours might influence the net magnetization field at the particle core. Such small core-core separations are, however, generally not a concern in MMUS when it comes to single core particles that are homogeneously dispersed. In these conditions, there dipole-dipole interactions are negligible, and each nanoparticle core will sense and react to the applied magnetization field independently.

1.2 Magnetomotive ultrasound

In MMUS, a time-varying magnetization field is applied to a region containing magnetic particles. When the field is active the particles will experience an attracting force towards the magnet. The force will set the particles and their surroundings in motion. When the field diminishes, so does the magnetic force and the particles will move back towards their original position dependent on the elasticity of the surroundings. Particle properties, and distribution, as well as the magnetic and mechanical properties of the surrounding material will determine the displacement. The magnetic nanoparticles experience a force towards the magnet, but hypothetically, a diamagnetic background material can reduce or even reverse the resulting motion, especially in regions with little or no magnetic particles.

The induced motion is detected with ultrasound, which is coherence based and therefore sensitive to axial motion. Under the assumption that any regions with a sufficiently high concentration of magnetic nanoparticles will move towards the magnet, the ultrasound data sequence can be processed to reveal those regions. A schematic overview of an MMUS system is shown in Fig. 6.

Although the magnetic nanoparticles themselves are too small to be directly detectable by ultrasound, their location can be inferred from the movement of the surrounding tissue.

As described herein in abridged form,⁶⁸ MMUS is a modality that may enable molecular imaging of extravascular targets, utilizing ultrasound with magnetic nanoparticles as a contrast agent. This is relevant to cancer

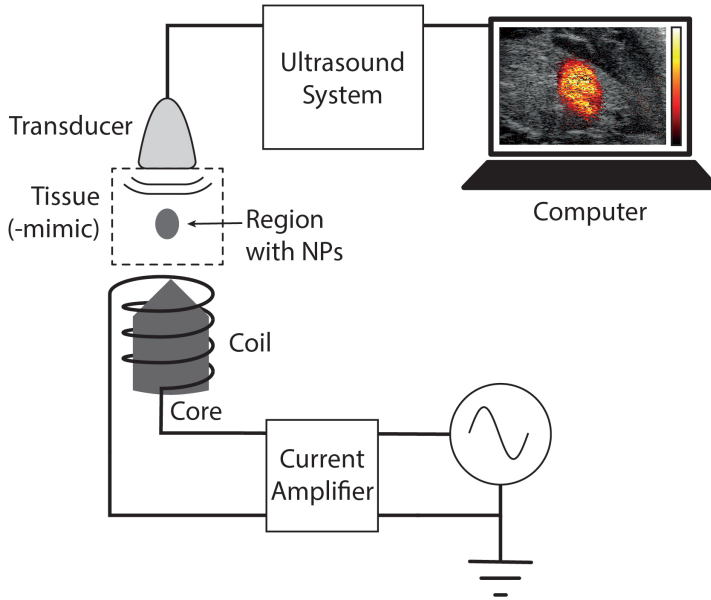


Figure 6: Schematic overview of an MMUS imaging system. The components of the imaging system: transducer, ultrasound machine, computer for data processing and display, are shown in the upper part of the figure. See also top right for an example MMUS image, reproduced with permission from.²² The principle of excitation is shown in the lower part of the figure, represented by a coil connected to a function generator via an amplifier. Note that the background material does not contain nanoparticles (NPs). The NP loaded region is shown as dark grey in the schematic, and is color coded in the example MMUS image.

imaging where soft tissue targets, for example lymph nodes, can be reached by the contrast agent for specific enhancement of these regions of interest.

1.3 Tissue mechanical properties

The contrast mechanism of MMUS relies on mechanical motion induced by a magnetic force. Magnitude and propagation of this motion depends on the tissue mechanical properties. Furthermore, such properties can be affected by disease progression and thereby contribute diagnostically relevant information.³⁵ Therefore, an overview of mechanical properties as they relate to magneto-mechanical interactions in soft tissue is included here.

Generally, if a force is applied to a region of a material the mechanical response follows the differential algebraic equation

$$\rho \frac{\partial^2 \mathbf{u}}{\partial t^2} = \text{div } \sigma + \mathbf{f}_V. \quad (7)$$

Here ρ is the (true) density, \mathbf{u} is the displacement field, div is the divergence operator, σ the stress tensor, and \mathbf{f}_V the volumetric force.

This equation can be readily applied to a collection of nanoparticles lodged in a material by considering their bulk properties. How stress and strain are related for a particular tissue can be represented by a material model.

Material models

Soft tissues generally respond to applied forces in a time dependent manner that can be characterized as viscoelastic. Viscoelasticity is a phenomenological approach of mechanical behavior, and does not represent the microscopic structure of the material. Material models are mathematical representations of materials that can be used to interpret, model or predict the outcome of mechanical perturbations.

A suitable model for a material can be determined based on experimental stress-strain data. Characterization is based on one or more mechanical tests. The results are not necessarily transferable to other conditions, for example temperature, strain rate and amplitude. It is therefore important to match the test conditions as closely as possible to the situation of interest.

In MMUS, the nanoparticle laden tissue is subjected to a time-varying, unidirectional magnetic force. For low frequencies,^{21,25} semi-static test conditions provide a good approximation. Some further differences between the mechanical test conditions and MMUS are worth noting. First, while MMUS may show displacements in the sub-micron range, the precision of commercial test machines is poor at such small perturbations⁷⁰ and so larger strains are used. Second, a force applied through magnetic interaction would not give rise to a uniform stress throughout the sample as is the case in compression testing. Considering this, a low strain semi-static compression test is expected to capture the material behavior under MMUS-like conditions.

A common test is stress-relaxation,⁶⁶ where a known strain is applied and the stress is measured as a function of time. Model selection is then based on

the characteristics of the relaxation curve. If the material dynamics differs with timescale, and this is important to account for, fractional models can be advantageous as they require few parameters to fit such data.⁶⁰ For simpler materials, the generalized Maxwell model, or GMM, provides a good fit to stress-relaxation data.⁷⁹ For the purpose of the slow-time magnetomotive response, the dynamics are dominated by the timescale of the excitation frequency, possibly superimposed on a transient relaxation. These conditions are handled by the GMM.

Once the model is determined, parameter values are estimated by fitting the model step response to the experimental data.

1.4 Microbubbles and their magnetic functionalization

Conventionally, exogenous ultrasound contrast is not achieved by magnetic excitation, but by micorbubbles. Microbubbles were first investigated as an ultrasound contrast agent (UCA) because they produce a strong echo.⁴¹ Early bubble suspensions were produced by agitating a saline solution,³⁰ thereby entraining gas in the liquid that would produce microbubbles at injection. The main limitation was that the gas would rapidly dissolve again into the surrounding liquid, resulting in a very limited duration.²⁰ There was therefore a need to improve microbubble stability before they could be used reliably as an ultrasound contrast agent.

Commercial preparations were developed for clinical use and introduced in the 1990's. An important property for estimating bubble stability is diffusion, thus the choice of gas will directly affect the time it takes for a bubble to dissolve.²⁰ While some commercial agents, like Levovist[®], do contain air, other gasses can be used to improve the survival. The gas cores of SonoVue[®] and Definity[®] contain heavy gasses with large molecular structures (Sulphur hexafluoride and Octafluoropropane respectively). Large molecules generally are less mobile, and thus have lower diffusivity which would act to extend the time until solution.

In addition to the selection of gas content, bubbles for ultrasound contrast are also stabilized by a shell, as illustrated in Fig. 7. SonoVue[®] and Definity[®] for example, are both contained by a lipid shell (with the addition of a surfactant in the latter case).

Although the rate of gas exchange can be influenced by the choice of gas and shell, change in the bubble diameter over time cannot be avoided. The level

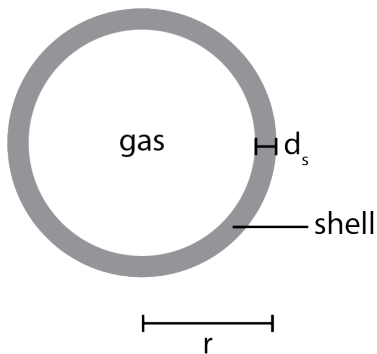


Figure 7: Schematic illustration of microbubble of radius r , stabilized by a shell of thickness d_s .

of gas saturation in the surrounding media strongly affects the persistence of bubbles, with a reduction in gas content by 10% reducing persistence by over 50%.⁵¹ Similarly, the behavior of suspended microbubbles is highly dependent on ambient temperature, since the shell is influenced to a greater and lesser extent depending on what material is used. Therefore phospholipid shelled microbubbles such as SonoVue[®] at room temperature, do not necessarily approximate what would be observed under *in vivo* conditions.⁵⁰

The fact that the stability of microbubbles is highly dependent on their surroundings highlights the importance of conducting *in vitro* experiments under relevant conditions if their results are to be relevant *in vivo*. The acoustic properties need to be controlled and kept stable in order for the bubbles to function well as an ultrasound contrast agent. The acoustic response depends largely on the size and mechanical properties of the bubble and its surroundings, which are both influenced during bubble degradation.

For example, the linear resonant frequency, f_r , is inversely dependent on the equilibrium bubble radius r . This resonance is also influenced by other factors of the gas, shell, and surrounding, such as the density of the surrounding medium ρ , the equilibrium pressure inside the microbubble p_e , the polytropic index of the gas κ , the shear modulus of the shell G_s , and instantaneous shell thickness d_s .³⁴

$$f_r = \frac{1}{2\pi r} \sqrt{\frac{3\kappa p_e + 12G_s \frac{d_s}{r}}{\rho}} \quad (8)$$

The shell that stabilizes the bubble thus also affects the acoustic response, such as the linear resonance frequency. It can also be functionalized to

different ends, such as drug delivery and targeting. This is not unique to microbubbles, but could be enhanced by sonoporation, which causes increased permeability of membranes near acoustically activated bubbles. It has been shown that sonoporation increases the occurrence of drug and genetic material delivery,⁵³ and can selectively and reversibly open the blood brain barrier.¹⁷ This therefore makes many targets available for delivery that are otherwise difficult to reach.

Other methods of bubble targeting include target-ligand binding, and magnetic attraction, each with different limitations. The probability of a binding event to take place increases the longer time the bubble can remain in proximity to the target. However, in physiological flow conditions, the agent is rapidly washed away and the incidence of binding is low. If bubbles are magnetically functionalized, an external static magnetic field can act to retain them against flow.⁵⁷ Magnetostatic attraction can in this way act to retain agents in the vicinity of targets, thereby increasing the chance of binding events.

Stable magnetic microbubbles can be produced by incorporation of iron oxide nanoparticles using different methods, see Fig 8. This can have an effect

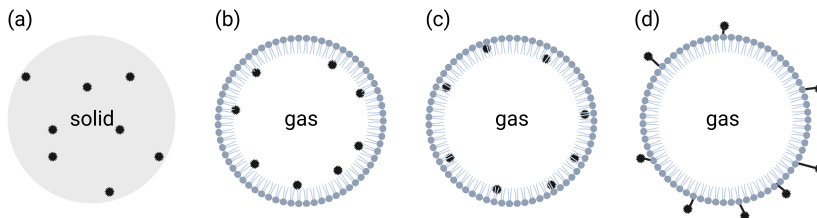


Figure 8: Schematic illustration of (a) an elastic solid containing homogenously distributed nanoparticles and (b-c) magnetic microbubbles containing magnetic nanoparticles that are confined to the shell. Depending on the method of microbubble fabrication, the particles can be (b) associated with the internal surface of the shell, (c) in the shell, or (d) on the external surface of the shell. Nanoparticles are represented as black, and the microbubble shells as consisting of phospholipids (with a hydrophilic head and two hydrophobic tails). Graphic created using BioRender.com

on the acoustic properties, for example if it leads to a change in diameter or thickness of the shell, see equation 8. The method of fabrication, or more specifically, where the magnetic nanoparticles are incorporated, affects the type and extent of any such acoustic modifications.⁹

Magnetic microbubbles have several interesting potential applications be-

yond targeting. Magnetomotive ultrasound (MMUS) is one example. MMUS uses the vibrations induced by an oscillating magnetic field to locate magnetic nanoparticles embedded in tissue. While the magnetic particles are usually introduced directly, incorporating them into bubbles could potentially improve the sensitivity of this technique. The spatial distribution of magnetic material is known to affect the displacement signal,⁴⁷ and in magnetic bubbles the magnetic material is typically constrained to the spherical surface. Additionally, the presence of gas would contribute to signal enhancement by providing excellent ultrasound contrast, and possibly facilitating motion.

Alternatively, the bubbles could act as a carrier and delivery system of the nanoparticle load. The sonoporation process previously mentioned can be utilized to enhance delivery of nanoparticles to an otherwise inaccessible area of interest. In this case, the bubbles would not be available to enhance sensitivity, and the MMUS sensitivity post destruction would depend on the delivered nanoparticle load.

Acoustic and mechanical properties of microbubbles is an active area of research, but low frequency magneto-mechanical interactions (in the order of Hz) are rather specific to the contrast enhanced MMUS application therefore of particular interest here. The magnetic force on a single magnetic microbubble depends on the iron loading. Core-core distance is also a factor, since closely packed nanoparticles may experience dipole-dipole interactions. For magnetic microbubbles, the core-core distance is influenced by iron loading, bubble size as well as particle size and composition. If the magnetic material is associated with the bubble shell,⁹ it can occupy a two dimensional surface with area A_s determined by the bubble radius. Furthermore, the mass of iron in one nanoparticle is given by

$$m_{Fe} = \gamma\rho V_c, \quad (9)$$

where volume fraction of iron in the core is γ , the density of iron ρ and the volume of the core is V_c

Volume fraction can be inferred from the composition of the core (the chemical formula describing the molar fractions of elements), and the corresponding atomic radii. There are different oxides of iron that can be used in magnetic nanoparticles, e.g. ferrite, Fe_2O_3 and magnetite, Fe_3O_4 . The volume fraction of iron in each of these oxides is approximated using the molar fractions and atomic radiiⁱⁱ, which are 140 pm for iron and 60 pm for oxygen.⁶⁹

ⁱⁱMetallic radii are different from atomic radii. This can be take in into account

The magnetic nanoparticles incorporated in a microbubble allows it to be manipulated by a magnetic force, and determines the magnitude of that force for certain field parameters. Once the bubble comes into contact with an interface, e.g. soft tissue, the arising deformations to both bubble and tissue are influenced by mechanical properties.

The magnetic microbubble can be represented as a thin shell surrounding a gaseous core. The initial pressure p_{in} of a gas is inversely proportional to the radius r_0 according to the Young-Laplace equation

$$P_{in} = 2\frac{\sigma}{r_0} \quad (10)$$

where σ is the surface tension of the bubble shell. The internal pressure, along with the mechanical properties of the shell, such as Young's modulus, Poisson's ratio and density, all contribute to the overall behavior of the bubble when exposed to an external force. The contact of a magnetic microbubble with an elastic solid can be modelled using finite element analysis for a specific set of these parameters, for a bubble with a certain size and shell thickness. Since the microbubbles are in the micrometer size range, but the shell can be only a few nanometers thick, the ratio of diameter to thickness is very large. This makes three-dimensional finite elements inappropriate. Instead, the shell can be modelled as a curved surface, using so called shell elements.

Interestingly, the contact between a magnetic microbubble and an elastic solid resembles a contact problem that has been solved analytically. Hertz contact theory describes the frictionless contact between an elastic sphere and an elastic half space.³³ Clearly, the analogy is a simplification, and in many cases, especially in an ultrasound field, the microbubbles are highly non-linear specifically due to the structure being inhomogeneous with a gas enclosed in a shell. For the magneto-mechanical interaction, however, the simplification may provide a useful theoretical foundation.

1.5 Cellular response

The movement in MMUS generally occurs in a delimited region, for example a lymph node, and with a movement amplitude in the micrometer range.

by using the Goldschmidt correction. The correction factor depends on the number of nearest neighbors (coordination number). For coordination numbers over six, the correction is less than 5%.⁴ The crystalline structures of ferrous oxides are complex,¹⁶ with coordination numbers mostly of six and over. Thus the correction between atomic and metallic radii would not change the results of this estimate substantially.

The movement is small compared to the tissue being imaged, and in relation to the resolution of ultrasound imaging systems, but comparable in size to many cells. Looking at the interactions between cells and nanoparticles under the influence of a varying magnetic force could provide insights into how the force is transferred from the particles to the tissue and how this process might affect cells.

The application of forces to cells has been studied extensively in the context of mechanical probing to infer viscoelastic properties,⁷⁷ as these can be linked to disease progression and treatment.⁶⁰ Depending on the method used, different structural components contribute to the measured mechanical properties.⁷⁷ When a low frequency modulated force is used the cytoskeletal contribution dominates.⁵⁹ Cellular response to mechanical stress is a complex process involving levels of signaling.⁴² Cyclic mechanical stimuli can elicit structural remodeling in endothelial cells⁶¹ and stress responses for example through reactive oxygen species, ROS.³⁶ Notably, mechanical stimuli are maintained for several hours before changes, such as reversible increased production of reactive oxygen species, are detected.¹³ In contrast, MMUS imaging only requires a modulated force to be applied for a fraction of this time.

Some cell types are sensitive to magnetic fields in the mT range, but with morphological changes occurring after several hours of exposure to a static,⁷² or low frequency field.^{29,28} Shorter exposure times reduce these effects.²⁸ It is not clear whether the relatively short exposure times associated with MMUS would have any measurable effect in this regard.

Cell models

Using cultured cells provides a simplified study system compared to the *in vivo* equivalent, and can make specific details accessible for observation. In this case, the details of interest are interactions between moving magnetic nanoparticles in living tissue and consequences thereof. Should these nanoparticles be feasible as a MMUS contrast agent, it needs to be ascertained if they are (a) taken up and (b) that they do not harm living cells.

Many cultured cells grow in adherent cell layers, which makes it possible to apply magnetic forces that can deform, but not freely translate them. This constitutes a simplified version of the tissues imaged by MMUS, where cells are not attached to a rigid surface, but to an extracellular matrix and

therefore mechanically constrained.

Uptake of iron oxide nanoparticles

Living cells need to exchange substances with the exterior to maintain their function and homeostasis. Mechanisms for uptake differ depending on the size and properties of the subject. Nanoparticles are by definition between 1 – 100 nm⁷³ and can be internalized through fluid phase endocytosis and receptor mediated internalization.⁵ Size is an important factor for nanoparticle transport *in vivo*^{37,24} and interactions with cells.²⁷ Smaller particles can penetrate more easily into tissues (eg. endothelium and cancerous tissue) but are also more rapidly cleared *in vivo*.⁶ Size dependent uptake favoring smaller particles has also been observed in cultured cells.¹⁹

Surface charge, or more precisely zeta potential, ζ , is another key feature determining uptake into cells.⁵ Dispersed particles with a surface charge will attract ions in the surrounding liquid. These ions form a layer of fluid that is attached around the particle. The zeta potential, ζ , is the electrical potential at the slipping plane, which is the interface between the attached liquid and the surrounding.⁴⁵ When suspended in biological media, iron oxide nanoparticles tend to adsorb proteins that form what is called a corona.² Corona formation drastically alters size and surface of nanomaterials which can completely dominate their behavior *in vivo*.⁷⁴ A negative zeta potential also promotes particle-cell interaction and uptake of dextran iron oxide nanoparticles into Caco-2 cells.⁵

Effects from particles, field and interactions

The nanoparticles and magneto-mechanical interactions that give MMUS its potential as a medical imaging tool need to be critically examined from a safety perspective.

While iron oxide nanoparticles at the concentrations used in here (Paper IV) typically do not directly affect viability, they may still alter the cell properties when internalized.⁴⁴ Indeed, certain effects can only be studied on a single cell level, since interactions with nanoparticles are not evenly distributed throughout a cell population.⁴⁸

Viability staining can be used to show how a treatment influences membrane function of individual cells. This is done by adding a dye, Trypan

blue. The dye cannot penetrate intact plasma membranes, so it only stains damaged cells. The proportion of damaged cells is determined by manual or automatic counting.

Alternatively, it is possible to detect substances escaping out through leaky membranes. Lactate dehydrogenase (LDH) is a stable enzyme present in most tissue types. It is normally found inside cells, mainly in the cytoplasm, and is involved in anaerobic metabolism²³ together with the cofactor Nicotinamide Adenine Dinucleotide, NAD^+ . LDH is released outside of the cell if the plasma membrane is damaged.

One method of testing membrane integrity of cultured cell populations is therefore to measure the level of LDH in the media. An advantage of this type of assay is that the cells can be continually cultured, since the test is only applied to the media.

While the specific physiochemical properties of nanomaterials may interfere with common cytotoxicity tests, the colorimetric LDH assay is generally reliable in the presence of iron oxide nanoparticles.³¹

Second, the level of reactive oxygen species indicates lower yet important stress experienced by the cells. Generation of reactive oxygen species (ROS) occurs at a controlled level in healthy cells.⁴⁹ Increased production occurs when cells are under oxidative stress, and the increased rate of oxidation can impair cell function.⁷¹ Oxidative damage is associated with a range of pathological conditions, including cancer⁴⁹ and potentially with mechanical stress.¹ Furthermore, increased ROS might contribute to increased malignancy in cancer.⁶⁷ It is therefore important to understand if the mechanical stresses that are generated during application of MMUS contribute to increasing ROS levels.

One dynamic indicator of oxidative stress is the ratio of reduced to oxidized glutathione, GSH:GSSG.³² GSH is abundant but in response to oxidative stress, some of it oxidizes into GSSG. Therefore, a reduction in this ratio is an indicator of oxidative stress.

Indicators of membrane damage and oxidative stress such as these have not previously been monitored in the context of MMUS. There is therefore a need to assess the cellular response to exposure to magnetic nanoparticles and forces applicable to these conditions.

2. Aims

MMUS is still in the pre-clinical phase and many aspects of in-depth understanding and development still remain before it can be clinically applicable. One interesting aspect of the technique that merits further exploration is the dependence of magnetomotion on the mechanical properties of the surrounding medium. The detected signal could therefore contain information not only about the particle distribution, but also of the tissue properties. This, in turn, could give clinically relevant information about tissue status.

Another aspect is the contrast agent itself. Up to now, magnetic nanoparticles have been used as a contrast agent in MMUS, but the particles can be configured in a more complex way, such as nanoclusters, to affect the magnetomotive signal. The particles can even be incorporated into microbubbles, which could allow for drug transport, magnetic retention and site-specific delivery using sonoporation. Magnetic microbubbles might thereby have some advantages as a contrast agent for MMUS.

All medical imaging systems involve some form of interaction with the tissue and with that a risk of adverse effects. While traditional ultrasound is generally considered a safe option, as it does not involve ionizing radiation, the added complexity of nanoparticles exhibiting mechanical motion in tissue warrants specific attention to establish the safety of the technique.

2. Aims

The above considerations therefore prompted the formulation of the following research questions (*RQs*).

RQ1 : How can the motion pattern in MMUS be characterized?

In particular,

- is finite element analysis a satisfactory characterization tool to do so?
- what is the role of diamagnetism?
- how does this relate to diagnosis?

RQ2 : Magnetic microbubbles have been suggested as a novel ultrasound contrast agent. What is the feasibility of magnetomotion in tissue induced by magnetic microbubbles? Theoretically,

- what kind of tissue displacements could magnetic manipulation of these microbubbles give rise to?
- which factors might affect the displacements, and in what way?

RQ3 : Are the magnetic nanoparticles and forces tolerated by live cells? Specifically,

- are the particles taken up by cells?
- what is the cellular response in terms of some relevant indicators?

The following sections expand on the methods used to answer these questions.

3. Materials and methods

The research questions have been addressed using a combination of inductive and deductive methodologies. Papers I and II use a combination of experimental and modelling approaches. Modelling is by definition a simplification of the physical system, and experimental data was used indirectly to decide how the model could be set up without oversimplification. Experimental data was also used directly as inputs to the model. The finite element model was set up to address RQ1, and to test the hypothesis about diamagnetism causing a counter motion. Papers I-II cover operating principle and theory that governs the motion, i.e. magnetic forces and mechanical properties of bulk materials that was included in the model. Modelling was also used in Paper III to address RQ2, but in this case aiming to develop a theory rather than testing one.

Fine scale dynamics regarding nanoparticle uptake, distribution, and the effects of magneto-mechanical forces were then explored in cultured cells (Paper IV). RQ3 was addressed in the planning stage of this study to determine suitable cells and indicators, and in the study where the response was investigated.

Methods were also selected in consideration of the 3Rs directive to replace, reduce and refine animal research [62]. While two of the papers (Paper 2 and 3) do contain animal data, these were collected in conjunction with other studies and were re-analyzed.

3.1 Tissue mimicking materials

Both oil-based gels and hydrogels were used. The oil-based gels were obtained by mixing styrene-ethylene-butylene-styrene (SEBS) and ballistics gel (Clear Ballistics LLC, Arizona, USA). Both of these gels are thermore-

versible, which means that they can be prepared separately and subsequently melted together to mix.

Polyvinyl alcohol (PVA), was used to form hydrogels. Briefly, PVA crystals were mixed with milli-Q water, then heated and maintained at 95°C until a homogeneous solution was formed. The solution was allowed to cool at room temperature. Graphite was added to the PVA solution to act as an ultrasound scatterer. Magnetic nanoparticles were added as appropriate, to act as a contrast agent for MMUS in delineated regions. The PVA components underwent two to three freeze-thaw cycles to obtain the desired instantaneous Young’s modulus.

3.2 Viscoelasticity

Stress-relaxation tests were performed using either of two mechanical testing machines (MTS Systems AB, Minnesota, USA or Bose 3100, Framingham, Massachusetts, U.S.). Briefly, samples were positioned and subjected to a small pre-load, before compression to the desired strain. The strain was then maintained for up to six minutes, over which period the force was recorded. The data were normalized by sample height and cross-sectional area to obtain stress-strain curves which were fitted to exponential functions derived from generalized Maxwell models, Fig. 9.

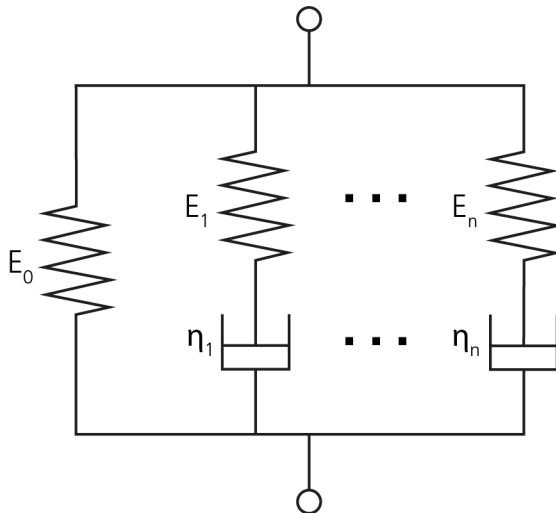


Figure 9: Generalized Maxwell model of viscoelasticity. Parameters E_0 through E_n represent the elastic contribution and η_1 through η_n the viscous contribution.

The resulting parameters were also used to estimate the instantaneous Young's modulus.

3.3 Finite element analysis

Geometries of an ultrasound phantom, lymph tissue, and a magnetic microbubble in contact with an elastic solid were created in a finite element analysis software (COMSOL Multiphysics v 5.5 or 5.6, COMSOL AB, Stockholm, Sweden), see Fig. 10.

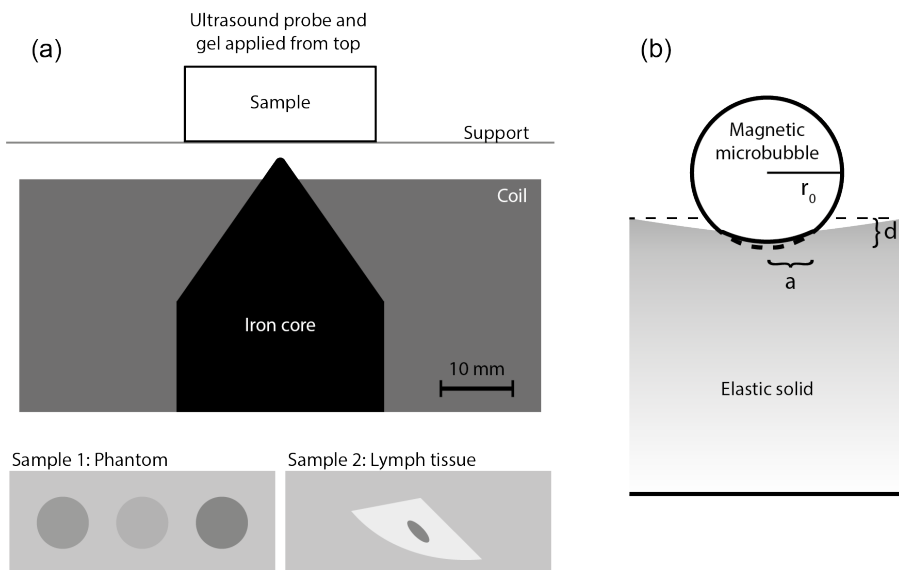


Figure 10: Geometries used in finite element analysis. A MMUS setup including the electromagnetic coil and iron core is shown in (a). Two different types of samples were modelled, shown below the main geometry. To the left a phantom with three inserts containing nanoparticles at different concentrations, illustrated by gray circles, and to the right lymph tissue, where the magnetic material was concentrated to the lymph node, shown in dark gray. A magnetic microbubble (b) was also modelled. The microbubble radius is r_0 and it comes into contact with an elastic solid such that the contact area has radius a and the deformation at the center is d .

The electromagnet was explicitly modelled to obtain a three-dimensional magnetization field. To model the magnetic coil and core, the geometry was made according to specifications of the electromagnet used for magnetomotive imaging. Material parameters were acquired from the literature. To estimate the coil wire cross sectional area, which was not known for

3. Materials and methods

this particular coil, a least squares fit was performed of measured field data to modelled magnetization field data for a range of areas. The fields were solved for using curl elements that lack higher derivatives. To access the first derivatives in the force calculation, see Equation 6 the solution was mapped onto Lagrangian elements. A partial differential equation on coefficient form was used for this mapping. The electromagnetic fields were solved for in the frequency domain given the input voltage to the electromagnet.

The force was then calculated from the modelled magnetization field using a Langevin function, Equation 5, scaled according to the nanoparticle suspension magnetization data and concentration, and the vector valued magnetic gradient force according to Equation 6.

The mechanical properties of the phantom material were modelled using a Generalized Maxwell model that takes elasticity and viscosity into account. For the elastic solid in the magnetic microbubble model, only (instantaneous) Young's modulus was used. For the phantom and lymph tissue models, a solid mechanics step was set up as a time dependent study. The solution from the electromagnetics step was used as an input for variables not solved for and only the solid mechanics interface was enabled. For the magnetic microbubble, a stationary analysis was used which was stabilized by an auxiliary sweep. The swept parameter controlled a spring foundation, the force and pressure, and was ramped up incrementally from zero to one.

The magnitude of the magnetic gradient force acting on a microbubble was estimated using field measurement conducted on the electromagnet, iron loading and data from the literature. For this case, the force was assumed to be evenly distributed over the shell.

To check whether dipole-dipole interactions might be important, the average interparticle distance was calculated. For a known iron loading, the average number of nanoparticles per microbubble can be calculated given the mass to number of nanoparticles conversion for a given suspension. The distance between adjacent particles was estimated by assuming that the surface of the shell can be segmented into equiareal circles with a nanoparticle at the center of eachⁱⁱⁱ. The expression for the interparticle distance, d is then twice the radius of such a circle with area a , calculated as the total

ⁱⁱⁱThere is extensive theory about the distribution of points on the surface of a sphere for the mathematically inclined.⁶³ For the purpose of this estimate, the distribution is not expected to be optimized in any way so an approximation suffices.

shell area A_s divided by the number of particles.

3.4 Magnetomotive ultrasound

Phantoms were imaged using a MS-250 transducer, with a center frequency of 21 MHz transducer with a preclinical ultrasound scanner (Vevo 2100, Visualsonics, Toronto, Canada). The transducer was positioned opposite the solenoid with the phantom between, with couplant gel providing acoustic contact with the probe as illustrated in Fig. 10. The solenoid, including a pointed iron core, was operated at 2.5 Hz through a function generator and amplifier (Behringer EP4000, Willich, Germany). Data was collected for 2 s at 58 fps. The data were transferred to a computer and post-processed²¹ with additional noise suppression to facilitate visualization where appropriate. Since some B-mode images contained dark regions, typically muscle tissue, these regions were masked to suppress phase noise.⁴⁰ The cut off was set to suppress pixels with less than 20% of the maximum B-mode intensity.

3.5 Cell-based assays

Two human-derived colorectal adenocarcinoma cell lines, HT-29 and Caco-2, were cultivated and exposed to magnetic nanoparticles and fields. These cells can be used to model the intestinal epithelium *in vitro*, which is relevant due to the interest in MMUS for colorectal cancer applications.

To quantify the iron retention in cells incubated with iron oxide nanoparticles a colorimetric method was used (ab83366, Abcam, Cambridge, England). Transmission Electron Microscopy (TEM) was then performed to further investigate qualitatively where particles accumulated.

Two assays additional assays were used to indicate cell membrane damage, LDH (ab65393, Abcam, Cambridge, England), and oxidative stress, GSH:GSSG (ab65393, Abcam, Cambridge, England), respectively.

LDH acts as a catalyst in a metabolic redox reaction. This catalytic property is exploited in colorimetric assays. There are two important steps in the reaction. The first step is a redox reaction catalyzed by LDH. Here NAD^+ is reduced to NADH. The second step involves a precursor, which is originally colorless but acts as a dye when reduced by NADH. The production

3. Materials and methods

of NADH, and subsequently the reduction of the precursor is proportional to the amount of LDH present.

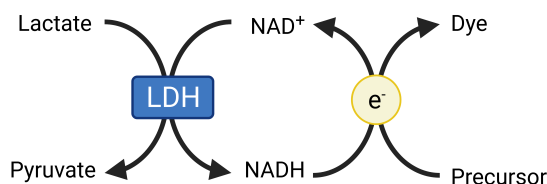


Figure 11: Reactions in LDH colorimetric assay. In the first reaction (left) LDH facilitates the production of NADH. The second reaction (right) changes the color of the precursor while oxidizing NADH. Diagram created using BioRender.com

The dye concentration is ascertained by measuring the absorbance at a specific wavelength.

The ratio of reduced to oxidized glutathione, GSH:GSSG is an indicator of oxidative stress level, and can be detected according to Fig. 12.

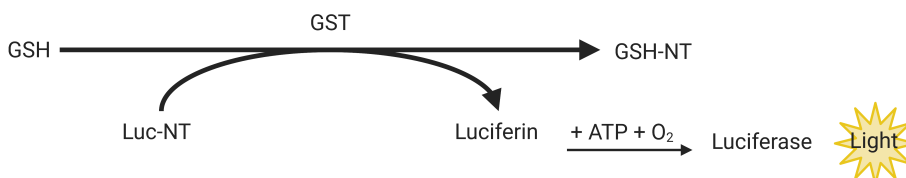


Figure 12: Reduced glutathione, GSH, can be detected using luminescence. To quantify the ratio of reduced to oxidized glutathione, GSH:GSSG using this reaction involves several steps. First, all glutathione in a sample is reduced to measure the total. Second, in a replicate sample the reduced glutathione is blocked, and remaining converted to the reduced state. Illustration created using BioRender.com

These indicators were measured in response to nanoparticles and/or the application of a time-varying magnetic force. The main outcomes, as well as their implications are discussed in the concluding sections.

4. Results and comments

Taken together, the papers presented in this dissertation illustrate the interplay between the magnetomotive technique and mechanical interaction on the tissue- and cellular level. They also illustrate how finite element analysis can be utilized to characterize and explore aspects of the study system, that would be difficult to investigate experimentally.

The research questions have all been addressed. In Papers I and II, the focus is on RQ1. Although the first paper does not explicitly refer to MMUS, it relates to acoustic and mechanical characterization, establishing methods that are applied again in Paper II where it was found that the motion pattern of MMUS can be explained by a finite element model that takes into account material properties. Interestingly, the countermotion that has been observed experimentally could not be fully explained by diamagnetism. Since the superparamagnetic contribution varies with magnetization according to Fig. 13, and the diamagnetic contribution increases linearly with magnetization field, the former tends to dominate at lower field strengths.

At higher field strengths however, saturation is reached and eventually the net magnetization will be diamagnetic. For magnetomotive optical coherence tomography, the limiting factor is penetration of light in tissue. The aim is therefore to image surface layers, and so the region of interest can be closer to the magnetic source than in MMUS, and the field strength higher. Under these circumstances, the diamagnetic contribution can become dominant. Furthermore, the higher resolution enables lower concentration of nanoparticles to be used, which again implicates that the diamagnetic contribution can become significant.

In MMUS on the other hand, the magnetization field is considered the limiting factor for imaging depth, and imaging plane extends into a small volume. In this case, the paramagnetic contribution is typically dominant.

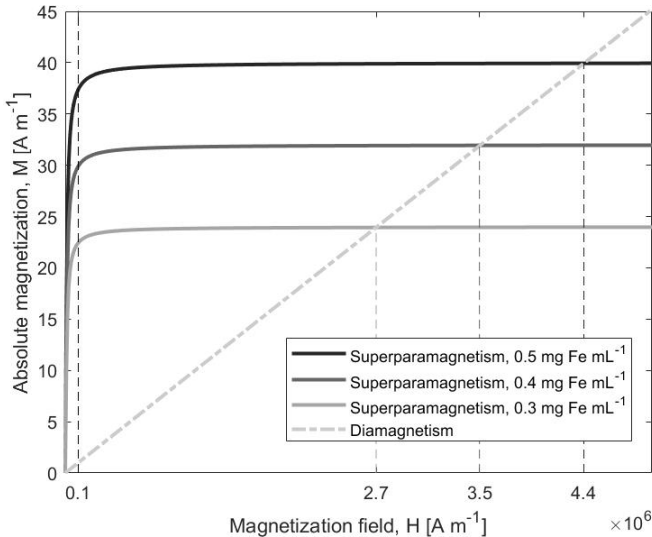


Figure 13: Magnetization due to diamagnetism of water and superparamagnetism of a nanoparticle suspension in three different concentrations.

In fact, for the field and particle parameters used in Paper II, 0.1 A m^{-1} and $0.3 - 0.5 \text{ mg Fe mL}^{-1}$, the superparamagnetic contribution was found to dominate by more than 20 fold, see Fig. 13 where the dashed vertical line intersects the lines representing the dia- and superparamagnetic contributions.

Furthermore, given the rapid decrease of the magnetization field with distance from the iron core tip, this effect would be even smaller in the particle free adjacent regions, where an opposing motion is sometimes observed. Consequently, such a motion cannot be fully explained by diamagnetism. Instead, the results of Paper II indicate conservation of mass, compressibility and boundary conditions as determining factors.

In Paper III, RQ2 and magnetic microbubbles are considered. The magneto-mechanical interactions of a magnetic microbubble with an elastic solid is explored using finite element analysis, as well as an analytical model for non-adhesive, elastic contact. Unlike MMUS using magnetic nanoparticles lodged in tissue, microbubbles are suspended in a liquid, and the magnetic material is associated with the bubble shell.

The interparticle distance was estimated for a set of magnetic microbubbles⁹ yielding distances according to Table 1.

Table 1: Approximate core separation in magnetic microbubble (MB) shells. Bubble and core diameter, d_b and d_c respectively, and iron loading are taken from.⁹ Nanoparticle (NP) separation is calculated as outlined in section 1.4.

d_b [μm]	d_c [nm]	Loading [pg Fe/MB]	NP separation [nm]
5.1	10	0.61	20
1.9	30	0.036	190
1.9	30	0.014	310
2.1	30	0.71	50

Consequently, for these parameters the core-core separation is $> 70 nm$ such that dipole-dipole interactions would be negligible⁷⁶ for two of the bubble types. However, in the first and last bubble listed, the separation is so small that these interactions would be important.

When attracted by a magnetic gradient force, the microbubble would come into contact with the boundary of the liquid domain, for example a lymphatic vessel. According to both methods, the magnetic bubble caused an indent in the elastic solid. Furthermore, the effect of some important variables, namely force magnitude, bubble radius and Young's modulus of the elastic solid were explicitly tested. Expressions using fractional exponents of these variables related each of them to for instance maximum displacement.

Finally, the cellular response to magnetic nanoparticles and forces (RQ3) was explored in Paper IV. During the planning stage of the study, several relevant indicators were identified from the literature. Two of these, LDH for membrane damage and GSH:GSSG for reactive oxygen species were evaluated. Two human colorectal cancer cell lines were selected as model systems, and uptake was confirmed in both.

TEM was used to image cells that were exposed to magnetic nanoparticles because it can resolve nanoscale details that would not be resolved by traditional light microscopy, see Fig. 14.

Each particle is made up of several smaller cores clustered together into particles resembling nanosized flowers, see Fig. 14 D.

The second cell line, Caco-2, was also found to take up the nanoparticles, see Fig. 15.

The results of the LDH and GSH:GSSG assays in Paper IV did not indicate adverse effects on these cells following exposure to MMUS conditions at moderate iron concentrations.

4. Results and comments

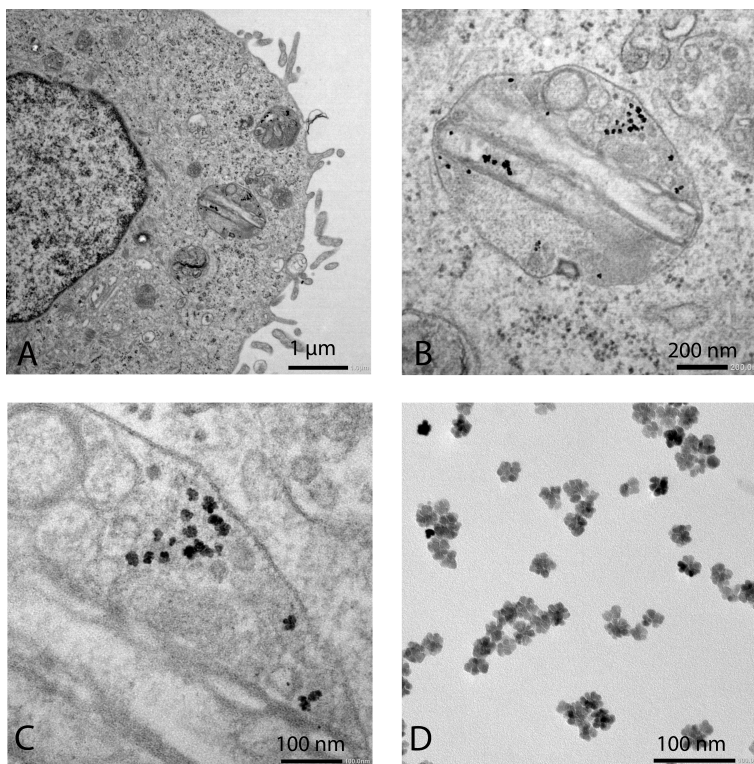


Figure 14: Transmission Electron Micrographs of part of a HT-29 cell that has been incubated with iron oxide nanoparticles (Synomag-D, plain, 50 nm, micromod Partikeltechnologie GmbH, Rostock, Germany) for 24 h. A collection of nanoparticles inside the cell are distinguishable from other structures and organelles by their characteristic shape and high contrast. The same region is shown with increasing magnification in panels A-C. The bottom right panel, D, shows the particles imaged in isolation as a comparison. Note that the scale bars of the individual subfigures represent $1\mu m$, $200nm$, $100nm$ and $100nm$ in A through D respectively.

There are several simplifications of the *in vitro* models compared to *in vivo*; The models are built up by a single cell type and they are grown on a two-dimensional surface, which is quite different from the physiological, three-dimensional tissue composed of several different types of cells supported by an extracellular matrix. Furthermore, since these cells are derived from cancerous tissues and are immortalized, meaning they can proliferate indefinitely, the results are not necessarily transferable to normal cells.

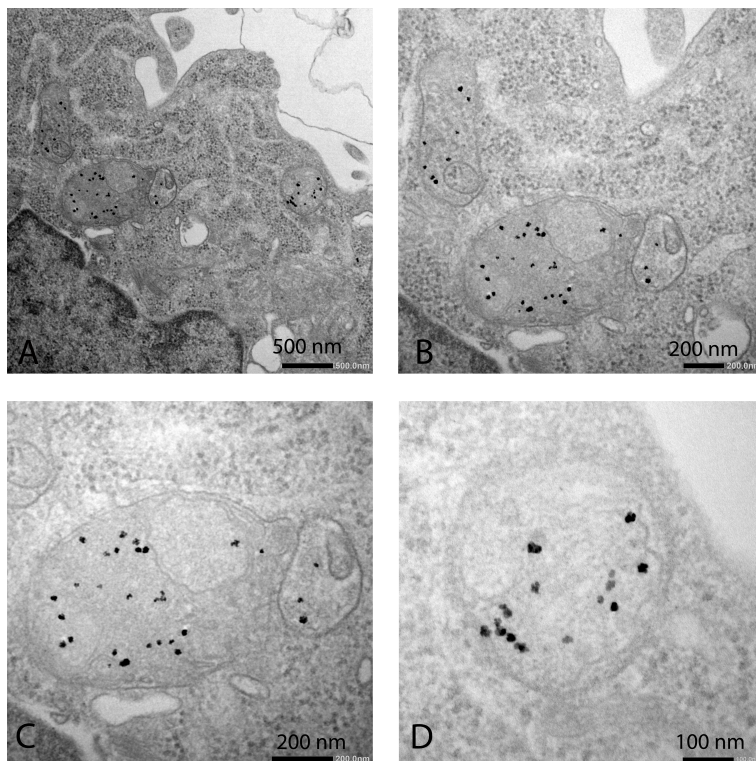


Figure 15: Transmission Electron Micrographs of part of a Caco-2 cell that has been incubated with iron oxide nanoparticles (Synomag-D, plain, 50 nm) for 24 h. Nanoparticles inside the cell are distinguishable by their shape and higher contrast. Parts of the region in A are shown with increased magnification in panels C-D. Note that the scale bars of the individual subfigures represent 500 nm, 200 nm, 200 nm and 100 nm in A through D respectively.

5. Implications and Outlook

Medical imaging is a powerful tool in cancer diagnostics, staging and treatment planning. New techniques and technical development can provide either more data, or more robust information. Development of imaging techniques to improve diagnostics is complex as it requires in-depth understanding of the different technical aspects, as well as of disease progression, *in vivo* systems and mechanisms, and clinical practice.

In the case of MMUS, there is a clear connection between the technical side of operating principle with a mechanical contrast mechanism, and the biological system where mechanical alterations can be linked to cancer progression. Therefore, it is relevant to use a mechanistic approach to this technique, that examines the study system based on these mechanical motions.

The mechanical properties of soft tissues are instrumental to this contrast mechanism. These can be evaluated *ex vivo* in compression or tensile testing, or *in vivo*, using for example sonoelastography. The phantom material with tunable viscoelasticity presented in Paper I could be of particular interest in sonoelasticity applications, as it is possible to obtain a range of different viscoelastic properties without the occurrence of speed-of-sound mismatch artifacts.

For MMUS specifically, both viscoelastic properties and compressibility influence the features of the images as outlined in Paper II. This implies that mechanical properties that are linked to cancer can be inferred from MMUS techniques, where contrast enhanced MMUS using magnetic microbubbles in Paper III, shows a similar potential. Even so, extracting the relevant information from MMUS images is not straightforward. Displacement patterns in MMUS are an amalgamation of properties of the tissues, contrast agents and setup, including tissue compressibility and viscoelasticity, speed of sound, contrast agent distribution and magnetic field strength. Increased

understanding of how different factors influence the resulting observed patterns can lead to a more accurate interpretation of different features.

In Paper IV, the cell-based safety evaluation was developed to gain some insights into whether these magnetic particles and forces would adversely affect living cells. It was found that the cell lines used, HT-29 and Caco-2, were prone to take up the nanoparticles. Cytotoxicity was somewhat increased by exposure to a high concentration of nanoparticles ($400 \mu\text{g Fe/mL}$), but no effect was observed at a lower concentration ($100 \mu\text{g Fe/mL}$). Furthermore, there was no evidence of adverse effects due to the nanoparticles in combination with a time-varying magnetic force.

The evaluation should not, however, be considered conclusive, as it was limited to two cell lines in 2-dimensional mono-cultures. To get a more comprehensive and realistic cell based model, co-cultures or 3-dimensional cultures can be used. The latter would also accommodate more magnetomotion, which might affect the cellular response. Furthermore, the response was categorized in terms of two important indicators of cell membrane damage and oxidative stress, LDH and GSH:GSSG. There are of course other indicators of adverse effects, such as formation of abasic sites in DNA (damage), or reduced barrier function, which can be assessed by transepithelial electrical resistance.

Taken together, the papers indicate that detection and evaluation of magnetomotion using different contrast agents can provide valuable diagnostic information. The preliminary cell based assessment also suggests that, for the cells and parameters tested, there is no significant negative response to the magnetic particles and force. This evaluation indicates an avenue for MMUS in cancer imaging.

6. References

- ¹ M. Ali, P. Mungai, and P. Schumacker. Stretch-induced phosphorylation of focal adhesion kinase in endothelial cells: Role of mitochondrial oxidants. *American Journal of Physiology - Lung Cellular and Molecular Physiology*, 291(1):L38–L45, 2006.
- ² R. Amalia, A. Adán, B. Lilianne, R. Carmen, G. Helena, M. Marzia, R.-R. Ildefonso, C. Sergio, M. Christopher J., and M. María del Puerto. Understanding the influence of a bifunctional polyethylene glycol derivative in protein corona formation around iron oxide nanoparticles. *Materials*, 12(14):2218, 2019.
- ³ B. Arnal, S. Yoon, J. Li, X. Gao, and M. O’Donnell. Magneto-optical nanoparticles for cyclic magnetomotive photoacoustic imaging. *Physica C: Superconductivity and its Applications*, 548:90–92, 2018.
- ⁴ P. Atkins and T. Overton. *Shriver and Atkins’ inorganic chemistry*. Oxford University Press, USA, 2010.
- ⁵ V. Ayala, A. P. Herrera, M. Latorre-Estevés, M. Torres-Lugo, and C. Rinaldi. Effect of surface charge on the colloidal stability and in vitro uptake of carboxymethyl dextran-coated iron oxide nanoparticles. *Journal of nanoparticle research : an interdisciplinary forum for nanoscale science and technology*, 15(8):1874, 2013.
- ⁶ S. Barua and S. Mitragotri. Review: Challenges associated with penetration of nanoparticles across cell and tissue barriers: A review of current status and future prospects. *Nano Today*, 9:223 – 243, 2014.
- ⁷ A. R. Bausch, W. Möller, and E. Sackmann. Measurement of local viscoelasticity and forces in living cells by magnetic tweezers. *Biophysical journal*, 76:573 – 579, 1999.
- ⁸ C. P. Bean and J. D. Livingston. Superparamagnetism. *Journal of Applied Physics*, 30(4):S120, 1959.
- ⁹ E. Beguin, L. Bau, S. Shrivastava, and E. Stride. Comparing strategies for magnetic functionalization of microbubbles. *ACS applied materials & interfaces*, 11(2):1829–1840, 2018.

6. REFERENCES

- ¹⁰ F. Bitter. The design of powerful electromagnets part i. the use of iron. *Review of Scientific Instruments*, 7(12):479–481, 1936.
- ¹¹ F. Bray, J. Ferlay, I. Soerjomataram, R. L. Siegel, L. A. Torre, and A. Jemal. Global cancer statistics 2018: Globocan estimates of incidence and mortality worldwide for 36 cancers in 185 countries. *CA: A Cancer Journal for Clinicians*, 68(6):394–424, 2018.
- ¹² A. C. Bruno, D. Sampaio, T. Pavan, O. Baffa, and A. A. Carneiro. A hybrid transducer to evaluate stomach emptying by ultrasound and susceptometric measurements: An in vivo feasibility study. *IEEE transactions on ultrasonics, ferroelectrics, and frequency control*, 62(7):1288–1294, 07 2015.
- ¹³ K. E. Chapman, S. E. Sinclair, D. Zhuang, A. Hassid, L. P. Desai, and C. M. Waters. Cyclic mechanical strain increases reactive oxygen species production in pulmonary epithelial cells. *American Journal of Physiology-Lung Cellular and Molecular Physiology*, 289(5):L834–L841, 2005.
- ¹⁴ J. P. Christiansen and J. R. Lindner. Molecular and cellular imaging with targeted contrast ultrasound. *Proceedings of the IEEE*, 93(4):809–818, April 2005.
- ¹⁵ R. Cobbold. *Foundations of Biomedical Ultrasound*. Biomedical engineering series. Oxford University Press, 2006.
- ¹⁶ R. M. Cornell and U. Schwertmann. *The iron oxides: structure, properties, reactions, occurrences and uses*. John Wiley & Sons, 2003.
- ¹⁷ A. Dasgupta, M. Liu, T. Ojha, G. Storm, F. Kiessling, and T. Lammers. Ultrasound-mediated drug delivery to the brain: principles, progress and prospects. *Drug Discovery Today: Technologies*, 20:41–48, 2016.
- ¹⁸ A. E. Deatsch and B. A. Evans. Heating efficiency in magnetic nanoparticle hyperthermia. *Journal of Magnetism and Magnetic Materials*, 354:163 – 172, 2014.
- ¹⁹ M. Enea, E. Pereira, D. D. Silva, J. Costa, M. E. Soares, M. de Lourdes Bastos, and H. Carmo. Study of the intestinal uptake and permeability of gold nanoparticles using both in vitro and in vivo approaches. *Nanotechnology*, 31(19):195102, 2020.
- ²⁰ P. S. Epstein and M. S. Plesset. On the stability of gas bubbles in liquid-gas solutions. *The Journal of Chemical Physics*, 18(11):1505–1509, 1950.
- ²¹ M. Evertsson, M. Cinthio, S. Fredriksson, F. Olsson, H. W. Persson, and T. Jansson. Frequency- and phase-sensitive magnetomotive ultrasound imaging of superparamagnetic iron oxide nanoparticles. *IEEE Transactions On Ultrasonics Ferroelectrics And Frequency Control*, (3):481, 2013.

-
- ²² M. Evertsson, M. Cinthio, P. Kjellman, S.-E. Strand, R. Andersson, T. Jansson, T. A. Tran, R. Zandt, G. Grafstrom, H. Toftevall, S. Fredriksson, and C. Ingvar. Combined magnetomotive ultrasound, pet/ct, and mr imaging of ga-68-labelled superparamagnetic iron oxide nanoparticles in rat sentinel lymph nodes in vivo. *Scientific reports*, 7, 2017.
- ²³ A. Farhana and S. L. Lappin. Biochemistry, lactate dehydrogenase (ldh). *Stat-Pearls [Internet]*, 2020.
- ²⁴ Q. Feng, K. Chen, J. Huang, K. Xiao, Y. Liu, and J. Huang. Uptake, distribution, clearance, and toxicity of iron oxide nanoparticles with different sizes and coatings. *Scientific Reports*, 8(1), 2018.
- ²⁵ M. Fink, M. Nuesslein, H. Ermert, S. Lyer, and C. Alexiou. Sonographic detection of magnetic nanoparticles for magnetic drug targeting in weak echogenic tissue. In *2015 IEEE International Ultrasonics Symposium (IUS)*, pages 1–6, Oct 2015.
- ²⁶ S. Frangos and J. R. Buscombe. Why should we be concerned about a "g"? *European journal of nuclear medicine and molecular imaging*, 46(2):519, 2019.
- ²⁷ N. Gal, A. Lassenberger, L. Herrero-Nogareda, A. Scheberl, E. Reimhult, V. Charwat, and C. Kasper. Interaction of size-tailored pegylated iron oxide nanoparticles with lipid membranes and cells. *ACS Biomaterials Science and Engineering*, 3(3):249–259, 2017.
- ²⁸ M. Girasole, A. Cricenti, R. Generosi, A. Congiu-Castellano, D. Pozzi, E. Pasquali, A. Lisi, and S. Grimaldi. Modifications of human lymphoblastoid cells induced by low-frequency magnetic field: A three-dimensional atomic-force microscopy study. *Applied Physics Letters*, 78(20):3145 – 3147, 2001.
- ²⁹ M. Girasole, A. Cricenti, R. Generosi, A. Congiu-Castellano, D. Pozzi, E. Pasquali, A. Lisi, N. Santoro, and S. Grimaldi. Atomic force microscopy study of lymphoblastoid cells under 50-hz 2-mt magnetic field irradiation. *Applied Physics A: Materials Science & Processing*, 67(2):219, 1998.
- ³⁰ R. Gramiak and P. M. Shah. Echocardiography of the aortic root. *Investigative radiology*, 3(5):356–366, 1968.
- ³¹ R. Guadagnini, B. H. Kenzaoui, L. Walker, G. Pojana, Z. Magdolenova, D. Bilanicova, M. Saunders, L. Juillerat-Jeanerret, A. Marcomini, A. Huk, M. Dusinska, L. M. Fjellsbø, F. Marano, and S. Boland. Toxicity screenings of nanomaterials: challenges due to interference with assay processes and components of classic in vitro tests. *Nanotoxicology*, 9(sup1):13–24, 2015.
- ³² P. Held. An introduction to reactive oxygen species measurement of ros in cells. 2010.
- ³³ H. Hertz. Über die berührung fester elastischer körper. *Journal für die reine und angewandte Mathematik*, 92:156–171, 1881.

6. REFERENCES

- ³⁴ L. Hoff, P. C. Sontum, and J. M. Hovem. Oscillations of polymeric microbubbles: Effect of the encapsulating shell. *The Journal of the Acoustical Society of America*, 107(4):2272–2280, 2000.
- ³⁵ M. T. Islam, S. Tang, C. Liverani, S. Saha, E. Tasciotti, and R. Righetti. Non-invasive imaging of young’s modulus and poisson’s ratio in cancers in vivo. *Scientific reports*, 10(1):1–12, 2020.
- ³⁶ Z. Kathrin S, R. Anjum, S. Hamid, L. Jia, T. Anders, and J. Staffan. The role of mechanical force and ros in integrin-dependent signals. *PLoS ONE*, 8(5):e64897, 2013.
- ³⁷ P. Kjellman, R. in ‘t Zandt, S. Fredriksson, and S.-E. Strand. Optimizing retention of multimodal imaging nanostructures in sentinel lymph nodes by nanoscale size tailoring. *Nanomedicine: Nanotechnology, Biology, and Medicine*, 10(5):e1089 – e1095, 2014.
- ³⁸ T. Kranemann, T. Ersepeke, S. Draack, and G. Schmitz. Modeling and measurement of the nonlinear force on nanoparticles in magnetomotive techniques. *IEEE Transactions on Ultrasonics, Ferroelectrics, and Frequency Control, Ultrasonics, Ferroelectrics, and Frequency Control, IEEE Transactions on, IEEE Trans. Ultrason., Ferroelect., Freq. Contr*, 67(4):679 – 690, 2020.
- ³⁹ G. M. Lanza, D. R. Abendschein, C. S. Hall, M. J. Scott, D. E. Scherrer, A. Houseman, J. G. Miller, and S. A. Wickline. In vivo molecular imaging of stretch-induced tissue factor in carotid arteries with ligand-targeted nanoparticles. *Journal of the American Society of Echocardiography*, 13(6):608 – 614, 2000.
- ⁴⁰ B. E. Levy and A. L. Oldenburg. Single magnetic particle motion in magnetomotive ultrasound: An analytical model and experimental validation. *IEEE Transactions on Ultrasonics, Ferroelectrics, and Frequency Control*, 2021.
- ⁴¹ J. R. Lindner. Microbubbles in medical imaging: current applications and future directions. *Nature reviews Drug discovery*, 3(6):527–533, 2004.
- ⁴² R. Lutz, T. Sakai, and M. Chiquet. Pericellular fibronectin is required for rho-dependent responses to cyclic strain in fibroblasts. *Journal of Cell Science*, 123(9):1511–1521, 2010.
- ⁴³ D. A. Mankoff, M. D. Farwell, A. S. Clark, and D. A. Pryma. Making molecular imaging a clinical tool for precision oncology: a review. *JAMA oncology*, 3(5):695–701, 2017.
- ⁴⁴ H. Mao, J. Li, I. Dulińska-Molak, N. Kawazoe, Y. Takeda, H. Mamiya, and G. Chen. Cellular effects of magnetic nanoparticles explored by atomic force microscopy. *Biomaterials science*, 3(9):1284 – 1290, 2015.
- ⁴⁵ A. D. McNaught, A. Wilkinson, et al. *Compendium of chemical terminology*, volume 1669. Blackwell Science Oxford, 1997.

-
- ⁴⁶ M. Mehrmohammadi, M. Qu, P. Kruizinga, R. Truby, S. Emelianov, T.-H. Shin, J.-H. Lee, and J. Cheon. In vivo pulsed magneto-motive ultrasound imaging using high-performance magnetoactive contrast nanoagents. *Nanoscale*, 5(22):11179–11186, 2013.
- ⁴⁷ M. Mehrmohammadi, K. Y. Yoon, M. Qu, K. P. Johnston, and S. Y. Emelianov. Enhanced pulsed magneto-motive ultrasound imaging using superparamagnetic nanoclusters. *Nanotechnology*, 22(4):045502, 2011.
- ⁴⁸ T. Meyer, T. Venus, H. Sieg, L. Böhmert, B. M. Kunz, B. Krause, P. Jalili, K. Hogeveen, S. Chevance, F. Gauffre, A. Burel, H. Jungnickel, J. Tentschert, P. Laux, A. Luch, A. Braeuning, A. Lampen, V. Fessard, J. Meijer, and I. Estrela-Lopis. Simultaneous quantification and visualization of titanium dioxide nanomaterial uptake at the single cell level in an in vitro model of the human small intestine. *Small Methods*, 3(5), 2019.
- ⁴⁹ K. Mokhtari, A. Pérez-Jiménez, L. García-Salguero, J. A. Lupiáñez, and E. E. Rufino-Palomares. Unveiling the differential antioxidant activity of maslinic acid in murine melanoma cells and in rat embryonic healthy cells following treatment with hydrogen peroxide. *Molecules (Basel, Switzerland)*, 25(17), 2020.
- ⁵⁰ H. Mulvana, E. Stride, J. V. Hajnal, and R. J. Eckersley. Temperature dependent behavior of ultrasound contrast agents. *Ultrasound in medicine & biology*, 36(6):925–934, 2010.
- ⁵¹ H. Mulvana, E. Stride, M.-X. Tang, J. V. Hajnal, and R. J. Eckersley. The influence of gas saturation on microbubble stability. *Ultrasound in medicine & biology*, 38(6):1097–1100, 2012.
- ⁵² J. L. Neuringer and R. E. Rosensweig. Ferrohydrodynamics. *The Physics of Fluids (1958-1988)*, 7(12):1927, 1964.
- ⁵³ M. Ogris, H. Sami, H. Dewitte, S. Roovers, S. C. De Smedt, I. Lentacker, and J. M. Walker. Enhancing nucleic acid delivery with ultrasound and microbubbles. *Nanotechnology for Nucleic Acid Delivery : Methods and Protocols*, page 241, 2019.
- ⁵⁴ J. Oh, M. D. Feldman, J. Kim, C. Condit, S. Emelianov, and T. E. Milner. Detection of magnetic nanoparticles in tissue using magneto-motive ultrasound. *Nanotechnology*, 17(16):4183 – 4190, 2006.
- ⁵⁵ A. L. Oldenburg, C. M. Gallippi, F. Tsui, T. C. Nichols, K. N. Beicker, R. K. Chhetri, D. Spivak, A. Richardson, and T. H. Fischer. Article: Magnetic and contrast properties of labeled platelets for magnetomotive optical coherence tomography. *Biophysical Journal*, 99:2374 – 2383, 2010.
- ⁵⁶ A. L. Oldenburg, J. R. Gunther, and S. A. Boppart. Imaging magnetically labeled cells with magnetomotive optical coherence tomography. *Optics Letters*, 30(7):747–749, Apr 2005.

6. REFERENCES

- ⁵⁷ J. Owen, C. Crake, J. Y. Lee, D. Carugo, E. Beguin, A. A. Khrapitchev, R. J. Browning, N. Sibson, and E. Stride. A versatile method for the preparation of particle-loaded microbubbles for multimodality imaging and targeted drug delivery. *Drug delivery and translational research*, 8(2):342–356, 2018.
- ⁵⁸ M. Qu, M. Mehrmohammadi, R. Truby, I. Graf, K. Homan, and S. Emelianov. Contrast-enhanced magneto-photo-acoustic imaging in vivo using dual-contrast nanoparticles. *Photoacoustics*, 2(2):55 – 62, 2014.
- ⁵⁹ L. Rebêlo, J. De Sousa, J. Filho, J. Schäpe, H. Doschke, and M. Radmacher. Microrheology of cells with magnetic force modulation atomic force microscopy. *Soft Matter*, 10(13):2141–2149, 2014.
- ⁶⁰ M. Rodríguez-Nieto, L. Montes-de Oca, G. Espinosa, P. Mendoza-Flores, P. Barrón-González, D. García-Ortiz, M. Mendoza-Villa, and J. Menchaca. Viscoelastic properties of doxorubicin-treated ht-29 cancer cells by atomic force microscopy: the fractional zener model as an optimal viscoelastic model for cells. *Biomechanics and Modeling in Mechanobiology*, 19(3):801–813, 2020.
- ⁶¹ K. Roland, N. Phu, U. Shunichi, and C. Shu. Cooperative effects of rho and mechanical stretch on stress fiber organization. *Proceedings of the National Academy of Sciences of the United States of America*, 102(44):15895, 2005.
- ⁶² W. M. S. Russell and R. L. Burch. *The principles of humane experimental technique*. Methuen, 1959.
- ⁶³ E. B. Saff and A. B. Kuijlaars. Distributing many points on a sphere. *The mathematical intelligencer*, 19(1):5–11, 1997.
- ⁶⁴ J. H. Scatliff and P. J. Morris. From röntgen to magnetic resonance imaging. *North Carolina Medical Journal*, 75(2):111–113, 2014.
- ⁶⁵ J. D. Schiffman, P. G. Fisher, and P. Gibbs. Early detection of cancer: past, present, and future. *American Society of Clinical Oncology Educational Book*, 35(1):57–65, 2015.
- ⁶⁶ F. Shama and P. Sherman. Stress relaxation during force-compression studies on foods with the instron universal testing machine and its implications. *Journal of Texture Studies*, 4(3):353, 1973.
- ⁶⁷ D. H. Shin, U. Dier, J. A. Melendez, and N. Hempel. Regulation of mmp-1 expression in response to hypoxia is dependent on the intracellular redox status of metastatic bladder cancer cells. *BBA - Molecular Basis of Disease*, 1852(12):2593 – 2602, 2015.
- ⁶⁸ S. Sjöstrand, M. Evertsson, and T. Jansson. Magnetomotive ultrasound imaging systems: Basic principles and first applications. *Ultrasound in Medicine and Biology*, 46(10):2636–2650, Oct. 2020.

-
- ⁶⁹ J. C. Slater. Atomic radii in crystals. *The Journal of Chemical Physics*, 41(10):3199–3204, 1964.
- ⁷⁰ TA Instruments. Electroforce 3100 test instrument. Brochure, 2015.
- ⁷¹ M. Takahashi, M. Shibata, and E. Niki. Estimation of lipid peroxidation of live cells using a fluorescent probe, diphenyl-1-pyrenylphosphine. *Free Radical Biology and Medicine*, 31(2):164 – 174, 2001.
- ⁷² L. Teodori, M. C. Albertini, F. Ugucioni, E. Falcieri, M. B. L. Rocchi, M. Battistelli, C. Coluzza, G. Piantanida, A. Bergamaschi, A. Magrini, R. Mucciato, and A. Accorsi. Static magnetic fields affect cell size, shape, orientation, and membrane surface of human glioblastoma cells, as demonstrated by electron, optic, and atomic force microscopy. *Cytometry. Part A : the journal of the International Society for Analytical Cytology*, 69(2):75 – 85, 2006.
- ⁷³ M. Vert, Y. Doi, K.-H. Hellwich, M. Hess, P. Hodge, P. Kubisa, M. Rinaudo, and F. Schué. Terminology for biorelated polymers and applications (iupac recommendations 2012). *Pure and Applied Chemistry*, 84(2):377–410, 2012.
- ⁷⁴ C. D. Walkey and W. C. W. Chan. Understanding and controlling the interaction of nanomaterials with proteins in a physiological environment. *Chemical Society reviews*, 41(7):2780 – 2799, 2012.
- ⁷⁵ World Health Organization. Global cancer observatory, 2021.
- ⁷⁶ K. Wu, D. Su, R. Saha, J. Liu, and J.-P. Wang. Investigating the effect of magnetic dipole–dipole interaction on magnetic particle spectroscopy: implications for magnetic nanoparticle-based bioassays and magnetic particle imaging. *Journal of Physics D: Applied Physics*, 52(33):335002, 2019.
- ⁷⁷ P.-H. Wu, D. R.-B. Aroush, A. Asnacios, W.-C. Chen, M. E. Dokukin, B. L. Doss, P. Durand-Smet, A. Ekpenyong, J. Guck, N. V. Guz, et al. A comparison of methods to assess cell mechanical properties. *Nature methods*, 15:491–498, 2018.
- ⁷⁸ M. Xu and L. V. Wang. Photoacoustic imaging in biomedicine. *Review of Scientific Instruments*, 77(4):041101, 2006.
- ⁷⁹ Q. Xu and B. Engquist. A mathematical and physical model improves accuracy in simulating solid material relaxation modulus and viscoelastic responses. 2014.
- ⁸⁰ J. Yu, H. N. Y. Nguyen, W. Steenbergen, and K. Kim. Recent development of technology and application of photoacoustic molecular imaging toward clinical translation. *Journal Of Nuclear Medicine: Official Publication, Society Of Nuclear Medicine*, 2018.

Research papers

Authors contributions

Co-authors that contributed to these papers are, listed alphabetically by last name: Roger Andersson, Esayas Atile, Marion Bacou, Luciana Carmago, Magnus Cinthio, Maria Evertsson, Susan Farrington, Lorenzo Grassi, Tomas Jansson, Katarzyna Kaczmarek, Benjamin Meirza, Carmel Moran, Susan Moug, Helen Mulvana, Theo Pavan, Sandra Sjöstrand, Ingrid Svensson, Adrian Thomson, Kathrin Zeller.

The authors own contributions to each paper are detailed below.

Paper I: Tuning viscoelasticity with minor changes in speed of sound in an ultrasound phantom material

Contributed to conception and design of the analysis. Collected data on speed of sound and density, and assisted in collecting stress-relaxation data. Analyzed speed of sound, density, stress-relaxation and attenuation data. Wrote and revised the paper with input from the co-authors.

Paper II: Displacement Patterns in Magnetomotive Ultrasound Explored by Finite Element Analysis

Developed a finite element model of the experimental setup, including the magnetic excitation coil and core, phantom material and lymph tissue. Collected data for some mechanical parameters needed for the model, and performed a literature search for the remaining material parameters. Implemented a filtering step to the and re-analyzed ultrasound data for mag-

netomotion. Originally drafted abstract, methods, results, discussion and conclusion, and revised the paper.

Paper III: Modelling of magnetic microbubbles to evaluate contrast enhanced magneto-motive ultrasound in lymph nodes – a pre-clinical study

Developed finite element models to simulate contact between a magnetic microbubble and an elastic solid. Interpreted the modelling outputs and related them to Hertz theory of contact. Collected MMUS data, implemented a more colorblind friendly scale and performed the analysis. Programmed and operated mechanical test machine. Analyzed the compression data. Drafted the manuscript.

Paper IV: Evaluation of cellular response in magnetomotive ultrasound

Suggested a collaboration and was involved in the application process to define and fund the project. Cultured cells from two human derived cell lines, performed the assays and programmed the microplate reader. Planned and prepared experimental work. Performed, assisted or instructed assay protocols. Collected samples for transmission electron microscopy. Participated (remotely due to restrictions) acquiring transmission electron microscopy images from ultra thin slices. Performed data analysis, presentation, drafted the manuscript.

